CHALMERS

Grip optimization in critical braking and cornering maneuvers using semi-active and active road vehicle suspensions

Master's thesis in Systems Control and Mechatronics

YIMENG LI

Department of Mechanics and Maritime Sciences
CHALMERS UNIVERSITY OF TECHNOLOGY
Göteborg, Sweden 2020

MASTER'S THESIS IN SYSTEMS CONTROL AND MECHATRONICS

Grip optimization in critical braking and cornering maneuvers using semi-active and active road vehicle suspensions

YIMENG LI

Department of Mechanics and Maritime Sciences
Division of Vehicle Engineering and Autonomous Systems
CHALMERS UNIVERSITY OF TECHNOLOGY

Göteborg, Sweden 2020

Grip optimization in critical braking and cornering maneuvers using semi-active and active road vehicle suspensions
YIMENG LI

Master's thesis 2020:45
Department of Mechanics and Maritime Sciences
Division of Vehicle Engineering and Autonomous Systems
Chalmers University of Technology
SE-412 96 Göteborg
Sweden
Telephone: +46 (0)31-772 1000

Cover:
Air suspension and semi-active dampers for the Volvo XC90

Chalmers Reproservice
Göteborg, Sweden 2020

Grip optimization in critical braking and cornering maneuvers using semi-active and active road vehicle suspensions
Master's thesis in Systems Control and Mechatronics
YIMENG LI
Department of Mechanics and Maritime Sciences
Division of Vehicle Engineering and Autonomous Systems
Chalmers University of Technology

Abstract

It is essential to optimize road holding in passenger cars for improving vehicle safety, especially in emergency situations. There are several factors that affect road holding: The material and texture of the tire contacting area with road; the vertical force pressing the contacting surface; and the friction of the road surface, et cetera. This study focuses on the influence of tire vertical force variation on the tire grip. Due to the lack of available sensors for tire vertical force, instead suspension system is controlled to affect the vertical tire force. By affecting ride comfort and handling performance, suspension is an important system that can ensure driving comfort by providing a sense of stability. Active and semi-active suspensions are nowadays often used to provide higher road grip since they can actively adjust damping force for different control objectives. This thesis investigates how both active and semi-active suspensions can be controlled to minimize the tire vertical force variation, and accordingly, improve the road grip. The main control objectives here are to minimize the tire vertical force variation and to improve the horizontal tire force generation ability. The tire performance in evasive maneuvers such as ABS braking is also discussed in this thesis. To simplify the problem, a quarter-car model with 2 degrees of freedom is developed and serves as the plant for control design. Three control strategies are developed and discussed: LQG control, active curve fitting control and compression maximization control. The first two controllers are separately tuned and applied to both active and semi-active suspensions, while the third one is only used for the semi-active damper. The performance of the developed controllers are evaluated in simulation and compared with passive suspensions. The overall improvements on the minimization of tire vertical force variation and the reduction of the braking distance are achieved. The tire grip can be considered improved in the case of emergency braking with only longitudinal maneuvers. Validation of the controlled systems performance for lateral tire force generation, and the driving test on real road, as well as further improvement of the control systems remain as future tasks.

Keywords: semi-active suspension, fully-active suspension, damper, LQG control, grip, braking

Preface

This study investigates the impact of controlling suspension systems on the tire grip optimization, which is of great significance for improving vehicle safety in emergency situations. The work includes system modelling, controller development, and simulation and analysis of the integrated vehicle systems. This study has been carried out from January 2020 to June 2020 and it was executed at Volvo Cars, Sweden. This thesis is supervised by Anton Albinsson and Johan Ericson, Volvo Cars and Mathias R Lidberg, Mechanics and Maritime Sciences, Chalmers University of Technology.

I would like to express my thanks to my industrial supervisors Anton Albinsson and Johan Ericson for their guidance and continous support through each stage of the process. I would like to acknowledge Mathias R Lidberg, my academic supervisor and examiner in Chalmers University of Technology, for helping me a lot regarding academic documentation and theoretical study throughout the thesis. Also, many thanks to Wolgan Dovland Herrera and Pontus Carlsson for their technical expertise and valuable advices. My student colleagues Dhurai Prabhahar and Mohammad Shaikh Ebrahim also gave me a lot of help, I am very grateful for this. Finally, I would like to thank my family for their support and accompany during this time period.

Gothenburg, June 2020

Yimeng Li

Nomenclature

Roman upper case letters

A	state matrix
B_1	input matrix
B_2	process noise matrix
C	output matrix
D	feedforward matrix
F_{damp}	damping force
F_{act}	active damper actuator force
$F_{dactive}$	active damper output damping force
F_b	braking force
$F_{control}$	controlled damping force
F_{dfit}	active curve fitting damping force
F_h	wheel center horizontal force
F_{rz}	vertical tire force
F_{dsemi}	semi-active damper output damping force
F_v	wheel center vertical force
F_x	longitudinal force
F_z	vertical force
H	height between the tyre surface and road surface
I_{min}	minimum control current
I_{max}	maximum control current
J	cost function variable
K	control feedback gain
L	tire contact length
L_{est}	estimation feedback gain
M	sweeping times
N	weighting parameter for correlation between states and control signal
P	Ricatti equation solution
Q	weighting parameter for states
R	weighting parameter for control signal
R_1	variance of process noise
R_{12}	covariance of process and measurement noise
R_2	variance of measurement noise
F_{rzRMS}	road grip
T_b	braking torque
W_o	observability matrix
W_r	controllability matrix
Z_r	tire vertical deflection

Z_s sprung mass vertical deflection

Z_u unsprung mass vertical deflection

Roman lower case letters

a_x longitudinal acceleration

a_z vertical unsprung mass acceleration

c_{sf} front suspension damping coefficient

c_{su} rear suspension damping coefficient

c_t wheel stiffness

c_u tire damping coefficient

d damping coefficient

d_B braking distance

d_{min} minimum damping coefficient

d_{max} maximum damping coefficient

f_d control signal for model state space representation

I_d damper current

k_{sr} rear suspension spring stiffness

k_{sf} front suspension spring stiffness

k_u tire spring stiffness

m_{sf} front wheel sprung mass

m_{sr} rear wheel sprung mass

m_{uf} front wheel unsprung mass

m_{ur} rear wheel unsprung mass

r reference signal

s_x tire slip

v damper deformation speed

v_d damper model velocity

v_m measurement noise

v_x vehicle lateral speed

w road waviness

$\hat{x}$ estimation states

y_{est} estimation measurement

y_{meas} measurement signal

Greek lower case letters

μ friction coefficient

μ_{brake} braking coefficient

Acronyms

ABS Anti-lock Braking System

ESC Electronic Stability Control

LQG Linear Quadratic Gaussian

LQR Linear Quadratic Regulator

LTI Linear Time-invariant

RMS Root Mean Square

WGN White Gaussian Noise

Contents

1 Introduction

This chapter presents the introduction of tire grip, the suspension system discussed in this project and the motivation behind this study. The project objective and the research questions are also formulated in this chapter. The implementation platform, the scope and delimitations are also discussed, and a brief summary of the content of each chapter is also presented here.

1.1 Background

The demands for vehicle safety motivates continuous improvement of vehicle performance. Main improvements can be obtained by electronic control systems with vehicle dynamics. Tire grip describes the contact interaction between the tire contact surface and the road surface, which plays an important role in affecting vehicle's performance in accelerating, cornering and braking. The deformation forces acting on the tire contact patch cause tire's global deformation, which results in a change in tire attainable global force. Since grip can be considered as the result of the tire generated friction force, improving tire grip is beneficial to improve the tire attainable global force. Since the maximal achievable acceleration is limited by the global force generated by the tires in evasive maneuvers such as Electronic Stability Control (ESC) intervention and Anti-lock braking system (ABS), by improving tire global force generation ability, more accidents can be potentially avoided. How to improve a vehicle's horizontal tire force generation under emergency situations is the main topic discussed in this study. Assuming the maximum tire friction coefficient is sensitive to the vertical tire force variation in the contact patch [13], by minimizing the tire vertical force variation the grip in the contact patch can be optimized [2].

Semi-active and active dampers are nowadays often used in suspension systems to improve vehicle's ride comfort or road holding. Beneficial from their characters of actively adjusting damping force, the controlled suspensions provide a high level of handling and driving comfort. In semi-active suspension systems, the parameters can be changed in a rather small time frame to dissipate or conserve the energy. However, the energy in active suspension systems can not only be both dissipated and conserved, but also can be collected into the system [15]. By adjusting the damping force of the wheel suspension system, the vertical tire force can be influenced. By electronically controlling the vertical suspension force through the damper of the suspension systems, the vehicle's performance in the case of emergency braking can be improved and accordingly, more collisions can potentially be prevented. There are relative researches discussing the control of semi-active suspension and active suspension systems. Niemz presented the development of a wheel load mini-max controller for semi-active suspension to maximize the tire vertical force. In this paper, the vertical tire load is directly measured and the effect of ABS system is also discussed to reduce the braking distance for a passenger car[15]. Xing et al. presented a work aiming at the vibration control for vehicle seat semi-active suspension system to improve ride comfort. In this paper, a Linear Quadratic Regulator (LQR) control strategy is investigated and applied to a magnetorheological semi-active damper[16]. Thanh et al. presented a work to enhance both ride comfort and road holding by using LQR control on active suspension. In this paper, an automobile half roll model is investigated and controlled system is compared with the passive suspension with hard and soft damping coefficient [12].

This project focuses on developing possible solutions on controlling both semi-active and active dampers to optimize the tire grip and to improve horizontal tire force generation ability. The research vehicle model will be provided by Volvo Cars and the implementation of the control algorithms will be conducted on Matlab /Simulink. To evaluate developed algorithms for the semi-active and active control, different road conditions such as uneven road are considered in the test. The performance of the control systems will be evaluated based on the measurement of the braking distance and the minimization of vertical force variation. The simulation tests are conducted on a vehicle simulation platform IPG carmaker.

1.2 Purpose

This thesis investigates both semi-active and active suspension systems and a few control methods including Linear Quadratic Gaussian control (LQG), active curve fitting control and compression maximization control are discussed to minimize the tire vertical force variation. Since in that case, the tire maximal attainable

global force can be improved and the vehicle performance in emergency situations can be improved. While maintaining vehicle stability, the improvement can be validated by the reduction of braking distance with full-brake applied.

1.3 Research questions

The objective of this thesis is to investigate the possibility of controlling the damping force for both semi-active suspension and active suspension systems to minimize the tire vertical force variation. Since braking distance provides information about all the quantities that influence the final result, like braking slip or braking force, reducing the braking distance is a measurable objective in this project. Besides, the longitudinal velocity of the vehicle at each time point is also of interest since if the time is too short to prevent an accident completely, it is still the consideration to decelerate the vehicle as much as possible.

The emergency braking with different evasive maneuvers is part of the investigation as well. With ABS, the objective is to trying to keep the braking slip at its optimal level. Since ESC applies asymmetrical brake to individual wheels to avoid possible loss of steering control, the objective is to maximize vertical force with changing brake force.

The braking performance of the vehicle in emergencies for different road surfaces is also considered in this project. It is possible not only to control damping to the needs of a given road, but also to react on unknown road's small bumps and holes. The developed suspension control algorithms are tested in the simulation with different road profiles to evaluate the adaptivity of the system to varying conditions.

1.4 Scope and Delimitations

By investigating how both semi-active and active systems can be controlled in emergency situations, the project aims at developing an optimal control algorithm to continuously control the dissipative vertical damper force for horizontal tire force maximization. Only one vehicle model is discussed in this thesis and the tire model is provided by the simulation platform. The analytical quarter car model is developed on Matlab/Simulink. The developed algorithm will be evaluated by simulating the controller behavior with the full vehicle model. Except for the testing maneuvers, the driving of the vehicle during simulations is controlled by the driver model itself. All results and conclusions of this thesis are representative for typical roads in real life, e.g. highways with a typical unevenness.

Deliverables

- Develop control algorithms for both semi-active and active systems.
- Validation of different control algorithms in the simulations.
- Tests of the developed algorithms for varying road profiles with braking and cornering maneuvers.

Delimitations

- Detailed vehicle models and other relative elements such as the influence of the driver and other parameters which might affect the vehicle's braking performance besides the vertical dynamics are out of considerations in this project.

1.5 Thesis Outline

This thesis presents the whole work of this study from Chapter 2. The theories behind the tire grip optimization and how it affects the braking process and the emergency safety are described in Chapter 2. There is also a description of the work theory behind the suspension systems which are controlled and investigated in this study.

Chapter 3 describes the vehicle system dynamics related to tire grip and the system model used for control

process. A quarter-car is modelled as the system plant, the state space representation of the plant model and the stability analysis of the built plant are presented in this chapter. The actuator model for semi-active and active dampers are also described here.

The implementation of the control strategies are described in Chapter 4. Three control strategies are investigated in this project, in which the LQG is mainly discussed in this study. The other two control methods active curve fitting and compression maximization control are implemented to compare their performance with the LQG control.

The parameters of the LQG controller and the evaluation process of the developed controllers are discussed in Chapter 5. Several types of road are used in the simulation. The simulation results and corresponding analysis are presented here.

Possible factors that affect the controller performance and corresponding improvement that can be conducted in the future are discussed in Chapter 6. Chapter 7 concludes this thesis and addresses possible future work based on the study results.

2 Braking the Suspended Wheel

2.1 Suspension system

Suspension system which connects a vehicle to its wheels plays an important role in affecting road grip and ride comfort. In order to improve road holding, semi-active suspension and active suspension systems are discussed. In comparison, passive suspension systems with soft and hard damping setting are also used as a reference.

2.1.1 Passive suspension system

Passive suspension system cannot provide extra energy to the suspension system. The passive suspension system limits its damping force to be calculated by a predefined damping coefficient for ride comfort or road holding. The damping coefficient d is defined by the rate between the damping force F_{damp} and the corresponding damper deformation speed v. Since the purpose of damping force is to dissipate the shocks coming to the vehicle body, its direction is opposite to the deformation velocity. The relation between the damping force and the deformation velocity can be formulated in Equation 2.1.

$$F_{damp} = -d \cdot v \tag{2.1}$$

There are two types of common used passive suspension systems. One is with nonlinear damping coefficient and the other is with a constant damping coefficient. But in a real car, only nonlinear damping coefficient are feasible. The two types of passive suspension systems are shown in Figure 2.1 and Figure 2.2.

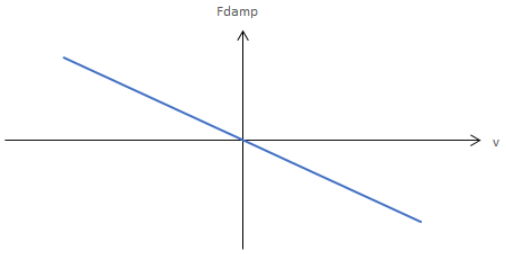

Figure 2.1: *Linear passive damper*

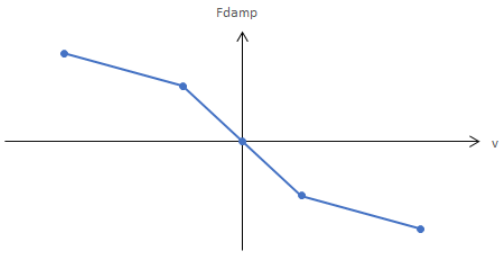

Figure 2.2: *Nonlinear passive damper*

2.1.2 Semi-active suspension system

Improved based on passive suspension system, the damping coefficient in semi-active suspension system can be tuned within certain amount of bandwidth while not adding energy into the system. Semi-active suspensions can adjust damping force of the shock absorber in real time, for different control objectives, in response to changing input wheel contact patch deflection [11]. However, semi-active suspension system limits the direction of the damping force to the opposite direction of the damping velocity. As shown in Figure 2.3, the shaded part is the operating field of the semi-active damper, the orange line and the blue line separately represents the upper limit and the lower limit of the possible output damping force. It also indicates the energy consumption range of the semi-active damper.

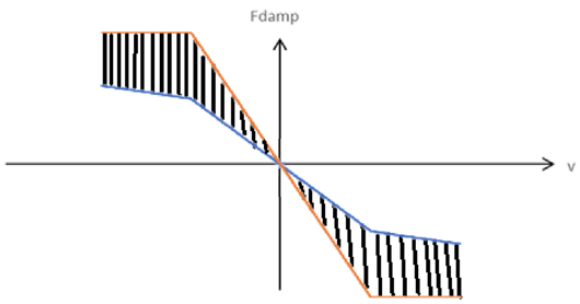

Figure 2.3: *Semi-active damper*

2.1.3 Active suspension system

Different from semi-active suspension, active suspension system can provide suspension force in both positive and negative directions of the damping velocity. As shown in Figure 2.4, the damping force can be generated in all four quadrants, where the 2nd and 4th quadrant indicate the energy exertion to this system. Using separate actuators, external force can be added into the suspension system to improve ride comfort or road holding [10]. Compared to semi-active suspension, fully active suspension system is more expensive and consumes more energy.

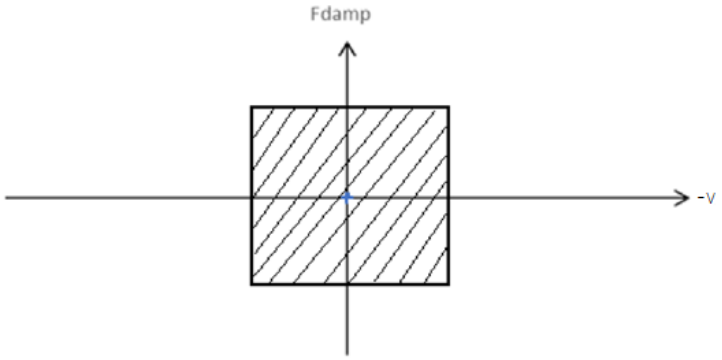

Figure 2.4: *Active damper*

2.2 Road grip

Grip is the force applied by one object to pull on or suspend from its contacting object. For vehicles, the grip, it is often referred to road grip or tire grip, describes the contact interaction between the tire contact patch and the road surface. Road grip plays an important role in providing ride safety for passengers. Road grip refers to the degree of retention of the longitudinal and lateral grip held between the tire and the road due to fixed vibrations when the vehicle is traveling on the road with a certain vertical unevenness at a certain speed [7]. Generally, there are several factors that can affect the road grip. For example, the material and texture of the tyre contact surface, the vertical force pressing the road contact surface, and the condition of the road surface will all affect the tyre road grip. However, since tyre mechanics is out of the discussion scope in this project, only the effect of the vertical tire force on the road grip is discussed.

Referring to [7], the road grip can be theoretically expressed in Equation 2.2, where F_{rzRMS} represents the road grip. This general expression is applicable for time domain measurement solutions.

$$F_{rzRMS} = RMS(\Delta F_{rz}(t)) \tag{2.2}$$

2.3 The braking process

A vehicle in motion has kinetic energy, and if the car is brought to stop, the kinetic energy must be removed. Braking is the process of controlling vehicle's speed by prohibiting its movement. The force to cause deceleration can be body force or the friction forces on the contact surface or the contact forces caused by the resistance of the car. The force distribution experience by a wheel during braking is shown in Figure 2.5, where F_z is the vertical tire force and F_b is the braking force. F_h and F_v represent the horizontal force and vertical force in wheel center. The vertical force is modelled in this study. The braking distance can be calculated by integrating the longitudinal velocity with respect to time, seen in Equation 2.3. If the braking torque increases, the longitudinal slip increases and therefore the longitudinal tire force increases [7]. With braking torque being constant, the degree of road grip at front and rear wheels plays an important role in affecting the tire force, and accordingly, vehicle's braking distance. Better road grip contributes to better braking performance. Therefore, braking distance could be used as a measurement to reflect the road grip conditions. In this project, braking maneuver is applied to the simulation of the controlled suspension systems. The braking distance can

be measured to evaluate the performance of the controlled systems in optimizing the road grip. As shown in Figure 2.5, it is clear that if and only if a braking slip occurs a braking force can be applied to the ground. In addition to manipulating the braking force by controlling the braking torque, the vertical force on the tire contact patch can also be controlled to affect the braking force, since the variation of the tire vertical force influences the horizontal tire force generation ability. The theory behind the influence is described in Section 2.4. The main purpose of braking in this project is to provide a maximum deceleration condition, so that the controlled system for grip optimization can make a contribution. Otherwise, the braking condition can be controlled by the driver, as is the braking distance. Therefore, only full-brake is applied in the braking tests.

$$d_B = \int_0^t v_x(t)dt \tag{2.3}$$

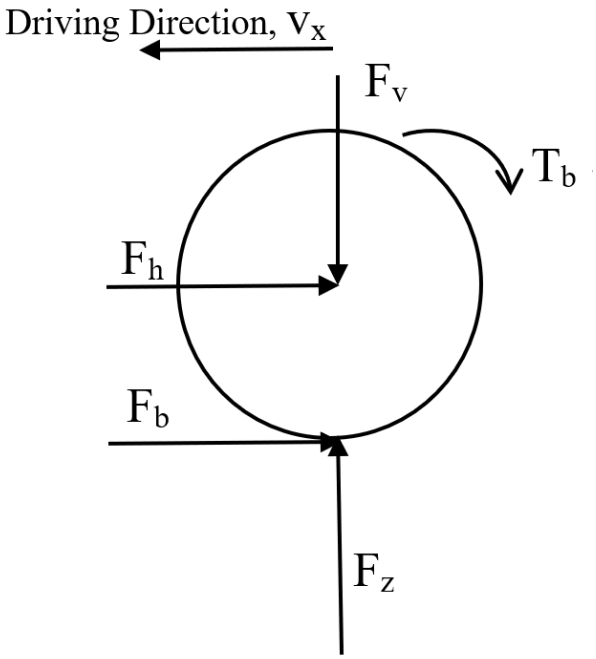

Figure 2.5: *Force distribution on a rolling wheel during braking*

2.4 Connecting wheel vertical displacement and braking slip

The braking force is essentially a longitudinal force F_x affected by the friction between the tire and road contact surface. From the longitudinal friction force-slip curve for a rolling wheel shown in Figure 2.6, it can be seen that the friction force has an initial linear region that builds to a peak value. After this peak is achieved, no further increase in the friction force is possible. Therefore, the longitudinal force F_x is limited by road friction. The maximum longitudinal force is achieved when the friction coefficient μ reaches the peak.

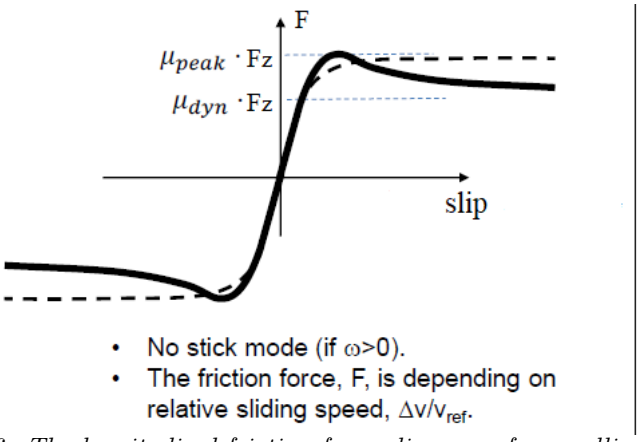

Figure 2.6: *The longitudinal friction force-slip curve for a rolling wheel[7]*

The calculation of the maximum longitudinal force is shown in Equation 2.4.

$$\max(F_x) = \mu F_z \tag{2.4}$$

The braking coefficient for a single wheel is defined as the ratio between the braking force and the vertical load. The calculation of braking coefficient μ_{brake} is shown in Equation 2.5. The μ_{brake} can be seen as a utilization of the friction coefficient, and the maximum value of μ_{brake} would never be higher than the friction coefficient. If the braking slip can be kept constant at the optimal value, an optimal braking performance can be reached.

$$\mu_{brake} = F_x/F_z \tag{2.5}$$

The longitudinal slip can be further explained by using the brush tire model. The tire module is shown in Figure 2.7. The shear stress is the tyre longitudinal stress in the brushes. It can be calculated with respect to tire slip s_x.

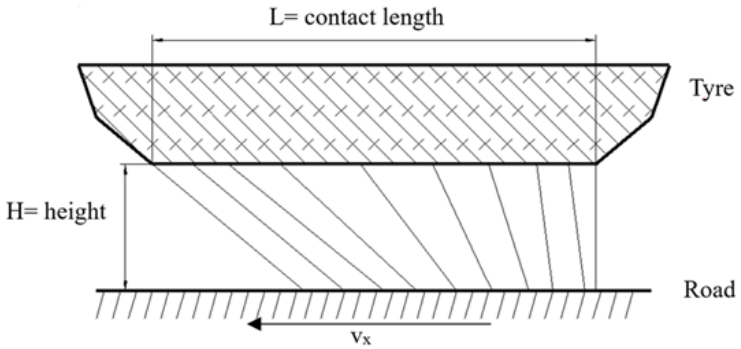

Figure 2.7: *Tire with tread element*

The longitudinal force F_x can be written as an integral of the shear stress. For the case friction limit is reached, the longitudinal force F_x reaches maximum and the calculation can be seen in Equation 2.4.

if the vertical force varies, it would be more difficult for a tyre to establish forces to the ground. When contact length varies, the resulting shear stress must restart from beginning again. As an average effect, the greater the change in vertical force, the tire will lose more and more grip [13]. By minimizing the variance of the vertical force F_z, which can be influenced by the vertical suspension force, the tire grip can be optimized and accordingly, the horizontal tire force generation ability can be improved and improves the vehicle performance during braking.

3 Vehicle System Dynamics

In this project, the quarter car system is investigated and modelled to describe the vehicle vertical dynamics. This chapter describes the modelling process of the quarter car mechanical system and the linear state space representation of the quarter car model. Besides, the actuator used in the suspension system is also modelled in this chapter.

3.1 Modelling of quarter car and suspension system

A 2 DOF quarter car model is studied in this project to analyze the vibration characters between road and wheel and between wheel and sprung mass. As shown in the Figure 3.1, a sprung mass m_s with 1 DOF is connected to an unsprung mass m_{us} through the suspension system, which is modelled as a linear spring and a damper. The tire is modelled also as a linear spring with damping, and it is always in contact with road surface. Both of the sprung and unsprung mass are driven by the excitation coming from the road profile z_c. The rational motion in wheel and body is neglected. Description of the variables and parameters in the quarter car model is shown in Nomenclature. The quarter car model with the suspension control is shown in Figure 3.1. The controller is added based on a passive damper, the value of the passive damping coefficient is chosen to be moderate hard and soft.

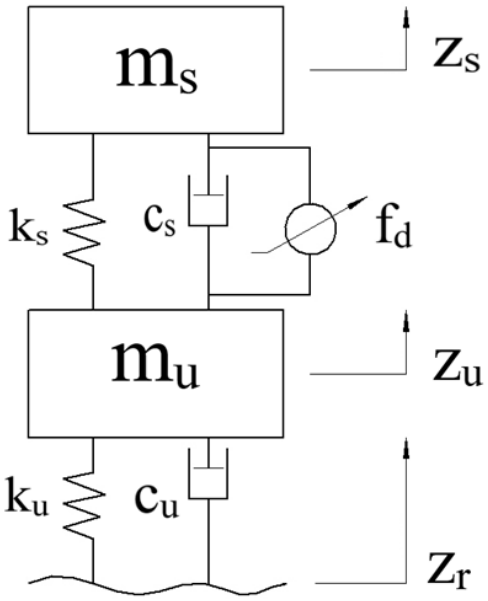

Figure 3.1: *The quarter-car model*

The equation of motion for the sprung mass can be written as:

$$m_s\ddot{Z}_s = -K_s(Z_s - Z_u) - C_s(\dot{Z}_s - \dot{Z}_u) \tag{3.1}$$

The equation of motion for the unsprung mass incorporate more elements as the unsprung mass is subject to the joint action of the upper and lower suspension forces, as well as the deformation from the road contact. The equation can be written as:

$$m_u\ddot{Z}_u = -K_t(Z_u - Z_r) - C_t(\dot{Z}_u - \dot{Z}_r) + C_s(\dot{Z}_s - \dot{Z}_u) + K_s(Z_s - Z_u) \tag{3.2}$$

3.2 State space representation and stability analysis

Ignoring the specific location of the wheels, the motion differential equations of the quarter car model are formalized in Equation 3.3, where f_d is the controlled damping force for the suspension system. In this problem, the tire displacement caused by road profile is considered as process disturbance in the state-space model.

$$\begin{cases} m_s\ddot{Z}_s = -K_s(Z_s - Z_u) - C_s(\dot{Z}_s - \dot{Z}_u) - f_d \\ m_u\ddot{Z}_u = -K_t(Z_u - Z_r) - C_t(\dot{Z}_u - \dot{Z}_r) + C_s(\dot{Z}_s - \dot{Z}_u) + f_d + K_s(Z_s - Z_u) \end{cases} \tag{3.3}$$

The states of this system and the system measurement are selected to be

$$x = [Z_u - Z_r, \dot{Z}_u, Z_s - Z_u, \dot{Z}_s] \qquad y = [Z_s - Z_u, \ddot{Z}_s] \tag{3.4}$$

The control signal in this system is:

$$u = f_d \tag{3.5}$$

The LTI state-space model can be derived from Equation 3.3. The generated state-space representation is shown in Equation 3.6, where w represents the process noise which in this case is the road profile disturbance, v_m represents the measurement noise.

$$\begin{cases} \dot{x} = Ax + B_1u + B_2w \\ y = Cx + Du + v_m \end{cases} \tag{3.6}$$

in which

$$A = \begin{bmatrix} 0 & 1 & 0 & 0 \\ \frac{-K_t}{m_u} & \frac{-C_t-C_s}{m_u} & \frac{K_s}{m_u} & \frac{C_s}{M_u} \\ 0 & -1 & 0 & 1 \\ 0 & \frac{C_s}{m_s} & \frac{-K_s}{m_s} & \frac{-C_s}{m_s} \end{bmatrix} \quad B_1 = \begin{bmatrix} 0 \\ \frac{1}{m_u} \\ 0 \\ -\frac{1}{m_s} \end{bmatrix} \quad B_2 = \begin{bmatrix} -1 \\ \frac{C_t}{m_u} \\ 0 \\ 0 \end{bmatrix} \tag{3.7}$$

$$C = \begin{bmatrix} 0 & 0 & 1 & 0 \\ 0 & \frac{C_s}{m_s} & \frac{-K_s}{m_s} & \frac{-C_s}{m_s} \end{bmatrix} \quad D = \begin{bmatrix} 0 \\ -\frac{1}{m_s} \end{bmatrix} \tag{3.8}$$

In order to design a LQR controller, the Linear time-invariant (LTI) system needs to be ensured stable, controllable and observable [8]. A LTI system is asymptotically stable if all eigenvalues of the system matrix A are located in the left half-plane. Since the eigenvalues of the matrix A are all negative in this quarter car model, the system can be considered asymptotically stable. A system is state controllable if any of its state origin can be reached in final time with the manipulations of external inputs. The controllability of this system is checked by the controllability matrix, which is given by Equation 3.9. The dimension of the controllability matrix is defined by the size of A and B_1, which is 4×4 in this project.

$$W_r = [B_1 \quad AB_1 \quad A^2B_1 \quad A^3B_1] \tag{3.9}$$

Since the controllability matrix W_r is not rank deficient, the system can be considered controllable.

Observability is a mathematical dual measurement of controllability to describe if any state of the system can be determined from the system measurements in finite time. The observability is checked though observability matrix, which is given by Equation 3.10. The dimension of the observability matrix is defined by the size of C and A, which is 8×4 in this project.

$$W_o = \begin{bmatrix} C \\ CA \\ CA^2 \\ CA^3 \end{bmatrix} \tag{3.10}$$

Since the observability matrix W_o is not rank deficient, the system can be considered observable.

3.3 Actuator Model

There are two types of actuator model used in this project. For each type, the same actuators are applied to four wheels. Both active and semi-active damper models are considered to be linear in this project. The final damping force equals to the summation of the controlled force and the predefined virtual passive damping force.

3.3.1 Active damper model

The active damper model used in this project is a black box model which is provided by the supplier. The structure of the damper model is shown in Figure 3.2. It takes the controlled force and the displacement of sprung and unsprung mass as inputs and outputs the damping force. The actuator has a limit on the output damping force. If the control force exceeds the maximum or minimum value, the active damper will act as a passive damper. The damping force determination process can be described in Equation 3.11 and Equation 3.12, where F_{act} is the actuator force determined by Z_s and Z_u and other configured parameters of the vehicle. $F_{control}$ is the controlled damping force and $F_{dactive}$ is the output damping force for the active damper model.

$$\begin{cases} Z_s \\ Z_u \end{cases} \rightarrow F_{act} \tag{3.11}$$

$$\begin{cases} |F_{act}| > |F_{control}| \rightarrow F_{dactive} = F_{control} \\ |F_{act}| < |F_{control}| \rightarrow F_{dactive} = F_{act} \end{cases} \tag{3.12}$$

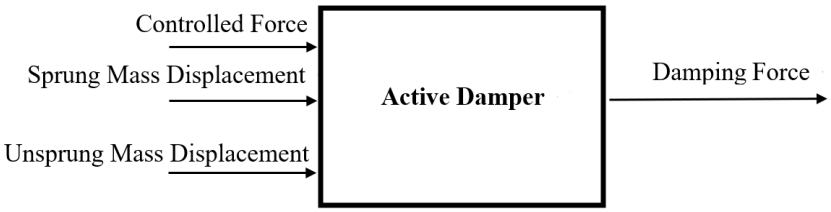

Figure 3.2: *The active damper model*

3.3.2 Semi-active damper model

The semi-active damper used in this project is a hydraulic actuated damper. By adjusting the control current, the oil flow can be adjusted actively to change the damping coefficient. In simulation, the damping force range for different damping velocity with certain control current is defined in a look-up table. The semi-active damper model is shown in Figure 3.3. It takes the control current and damping velocity as input and outputs the damping force to the suspension system. Equation 3.13 shows the dependencies of the input and output parameters, where I_d is the damper current, d and v_d are the damping coefficient and damper velocity. F_{dsemi} is the output damping force for the semi-active damper model. By using different I_d, the damper coefficient d can be tuned. According to Equation 2.1, the damping force for the semi-active damper model can be calculated based on the damper coefficient and damper velocity.

$$\begin{aligned} I_d &\xrightarrow{tune} d \\ F_{dsemi} &= -d \cdot v_d \end{aligned} \tag{3.13}$$

Figure 3.3: *The semi-active damper model*

4 Control Design

This thesis studies three control strategies, namely LQG controller, active curve fitting control and compression maximization control strategy. The implementation process of the three controllers are discussed in this chapter. The design parameters for the LQG controller such as weight matrix and observer gain were tuned and determined for the fully active suspension system. The LQG controller is also applied to the semi-active suspension system. But the weight parameters are separately tuned based on the that for the fully active suspension. The LQG control is the main control method discussed here, the other two possible solutions for grip optimization are investigated to compare and analyze their performances with the LQG control. The simulations and analysis are presented in Chapter 5.

4.1 Optimal control theory

Optimal control strategy is a mathematical optimization method which aims at deriving control policies for a given dynamic systems such that a certain optimality criterion is achieved. A control problem includes a cost function that is a function of state and control variables. An optimal control is a set of different equations describing the paths of the control variables that minimize the cost function [8]. The optimal control theory is applied to the LQG control method and the control part of the LQG control is discussed in Subsection 4.1.1.

4.1.1 Linear quadratic regulator

Linear Quadratic Regulator (LQR) is an optimal control method which provides optimal feedback gain to generate the control signal to the plant. The LQR operates based on model-based system by minimizing a cost function. For a continuous time linear system defined as

$$\dot{x}(t) = Ax(t) + Bu(t) \tag{4.1}$$

the typical form of cost function for solving LQR problem can be generated as:

$$J = \int_0^\infty (x^\intercal Q x + u^\intercal R u + 2x^\intercal N u) dt \tag{4.2}$$

where Q, R and N are positive definite weighting matrix. To minimize the cost function J, the state feedback control law is introduced.

$$u = -Kx \tag{4.3}$$

The feedback gain K can be calculated through Equation 4.4, where $P \geq 0$ and is a symmetric variable. By solving the Riccati Equation 4.5, P can be calculated, the LQR gain K can be obtained [8].

$$K = R^{-1}(B^\intercal P + N^\intercal) \tag{4.4}$$

$$0 = A^\intercal P + PA + Q - (PB + N)R^{-1}(PB + N)^\intercal \tag{4.5}$$

The optimal closed-loop feedback system can now be generated as:

$$\dot{x} = (A - BK)x \tag{4.6}$$

A general structure of the LQR control system is shown in Figure 4.1, in which r is the reference signal to this system and y is the measurement signal.

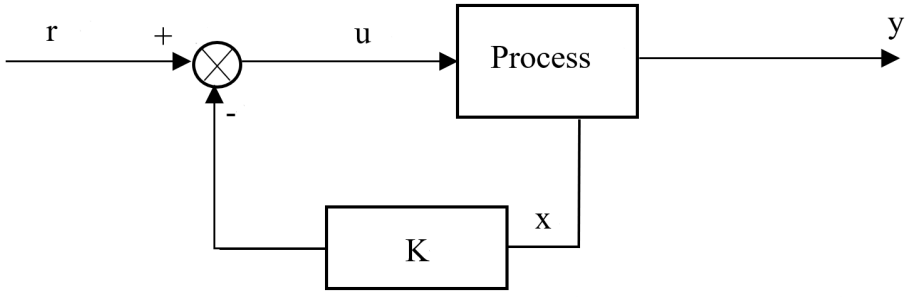

Figure 4.1: *The structure of LQR control*

By choosing different value for Q and R, LQR is able to find a trade-off between states penalization and control effort. The larger these values are, the more penalties for these signals. Generally, choosing a large value for R means penalizing more on the control signal, the control strategy is expensive. On the contrary, small value for R results in cheap control strategy. Similarly, choosing a large value for Q means the it is trying to stablize the system with the least state errors, while a large Q means less attention to the state errors. The Q and R matrix are in the form stated in Equation 4.7 and Equation 4.8.

$$Q = \begin{bmatrix} q_1 & 0 & 0 & 0 \\ 0 & q_2 & 0 & 0 \\ 0 & 0 & q_3 & 0 \\ 0 & 0 & 0 & q_4 \end{bmatrix} \tag{4.7}$$

$$R = r_1 \tag{4.8}$$

4.2 LQG implementation

Since the LQG control consists of a state observer and a LQR controller and it requires full state feedback, the implementation of the LQG controller is divided into two parts: the design of state observer and the determination of weight matrix. This section discusses the two processes separately for fully active suspension and semi-active suspension systems.

4.2.1 Observer design

Given the system is observable, It is possible to design an observer to estimate the system states. Limited by the applied sensors on the vehicle, some of the states are not measurable. By using the separation principle [3], the state estimates can be used for the state feedback controller as the input to generate a regulator for the system.

Based on the developed quarter car state space model, the state estimate has the form:

$$\begin{aligned} \hat{x} &= A\hat{x} + B_1 u + B_2 w + L_{est}(y - \hat{y}) \\ \hat{y} &= C\hat{x} + Du \end{aligned} \tag{4.9}$$

in which L_{est} is the observer gain. In this project, the observer gain is obtained by applying a Kalman state estimator, which can provide the optimal gain solution given process and measurement noise covariance.

By solving an algebraic Ricatti Equation 4.10, the observer gain can be calculated in Equation 5.2:

$$0 = AP + PA^\intercal - (PC^\intercal + NR_{12})R_2^{-1}(PC^\intercal + NR_{12})^\intercal + NR_1N^\intercal \tag{4.10}$$

$$L_{est} = (PC^\intercal + NR_{12})R_2^{-1} \tag{4.11}$$

where P is positive and symmetric that equals the minimum state estimation error covariance, which can be seen in Equation 4.12.

$$P = E\{(x(t) - \hat{x}(t))(x(t) - \hat{x}(t))^\intercal\} \tag{4.12}$$

The process and measurement noise introduced in Equation 3.6 are chosen to be independent white Gaussian noise:

$$\begin{bmatrix} w \\ v_m \end{bmatrix} \sim WGN\left(0, \begin{bmatrix} R_1 & 0 \\ 0 & R_2 \end{bmatrix}\right) \tag{4.13}$$

4.2.2 active suspension

According to the control objective of minimizing the tire vertical force variation to optimize the tire grip, all variables of the state vector are taken into account. Since there is no available sensor for the tire vertical force and the force is hard to estimate, the vertical suspension force variation becomes the control objective for the

tuning of the design parameters. The system performance function for a quarter car model is formulated as follows:

$$J = \int_0^\infty (\rho_1(Z_u - Z_r)^2 + \rho_2 \dot{Z}_u^2 + \rho_3(Z_s - Z_u)^2 + \rho_4 \dot{Z}_s^2 + r_1 f_d^2) \tag{4.14}$$

in which $\rho_1, \rho_2, \rho_3, \rho_4$ and r_1 are the weighting parameters of the cost function. Accordingly, the weight matrix are defined as:

$$Q = \begin{bmatrix} \rho_1 & 0 & 0 & 0 \\ 0 & \rho_2 & 0 & 0 \\ 0 & 0 & \rho_3 & 0 \\ 0 & 0 & 0 & \rho_4 \end{bmatrix} \quad R = r_1 \quad N = \begin{bmatrix} 0 \\ 0 \\ 0 \\ 0 \end{bmatrix} \tag{4.15}$$

Since our purpose is to minimize the wheel vertical force, the penalization mainly focus on the two deflection states $(Z_u - Z_r)$ and $(Z_s - Z_u)$, and also the velocity of the unsprung mass $\dot{Z}_u$. Since penalizing the control signal is not a demand in the control purpose, a small value is chosen for R. During the weighting tuning process, the third parameter of N matrix is found to be effective in minimizing the wheel vertical acceleration, so it is also given a certain penalization. The determined parameter values are shown in Chapter 5. The structure of the LQG control system for the quarter car model can be seen in Figure 4.2, in which the control input can be calculated in Equation 4.16:

$$\begin{aligned} \hat{x} &= A\hat{x} + Bu + Gw + L_{est}\underbrace{(y_{meas} - y_{est})}_{error} \\ u &= -K\hat{x} \end{aligned} \tag{4.16}$$

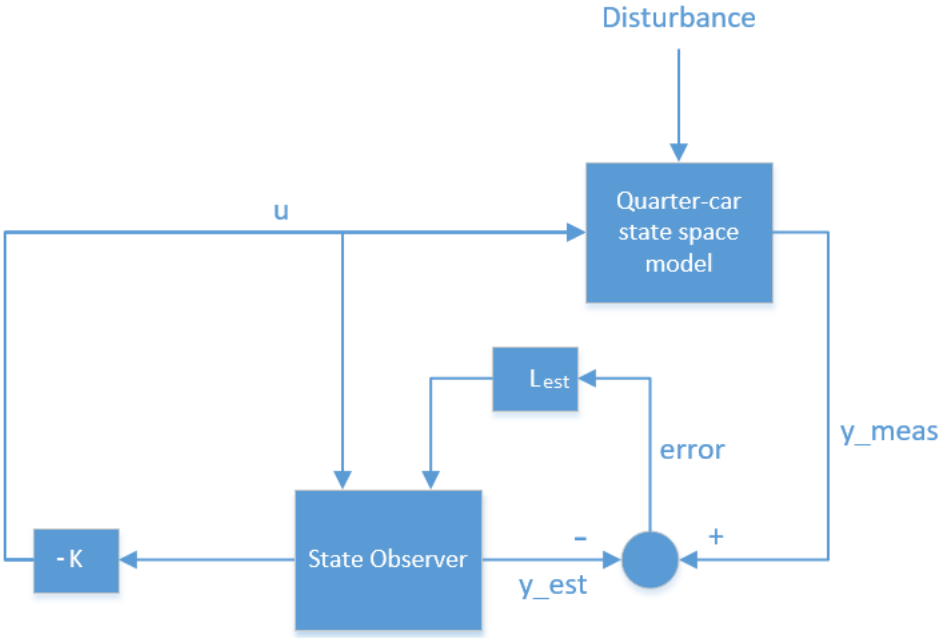

Figure 4.2: *The structure of the LQR control system*

4.2.3 semi-active suspension

The LQG controller for semi-active suspension can be modified based on the controller for fully-active suspension. Since limited by the energy consumption, the weighting parameters for fully-active damper may not be optimal for the system with semi-active damper. Through a round of rial and error, the modified weighting parameters Q, R and N are shown in Chapter 5.

For the semi-active suspension, as limited by energy exertion, the damping force output from the LQG controller cannot be always reached. Therefore, a damping force - current converter is needed to produce an

linear interpolated damping current. The relation between the damper velocity, control current and damping force for the semi-active damper are plotted in Figure 4.3 and Figure 4.4. The damping force - current converter takes the damper velocity and control force as input. By locating the current damper velocity to the three current levels, a set of query points can be obtained. Inserting the query points to the damping force-velocity look-up table of the semi-active damper, the corresponding damping force for each current level can be generated. For the case that the damping force the semi-active damper can provide is less than the force output from the LQG controller, or the LQG force is too small and out of the range of the possible damping force the semi-active damper can provide with the current damper velocity, the damping force will be updated and assigned to the maximum or the minimum of the generated force. Otherwise, the damping force will keep its original value. Through linear interpolation, the final current which best describes the required damping force can be determined. An example of the final interpolated current signal is shown in Figure 4.5.

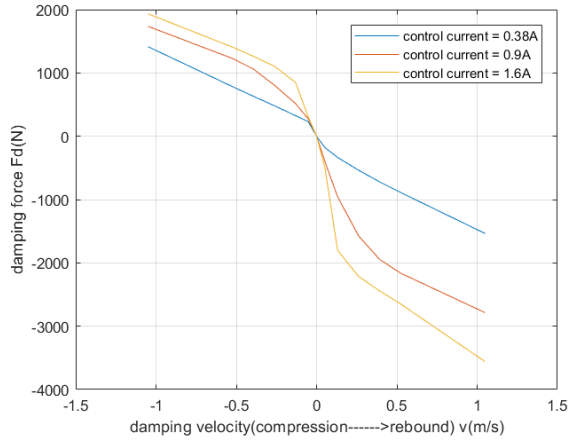

Figure 4.3: *Front damping force vs damper velocity for different control currents for the semi-active damper*

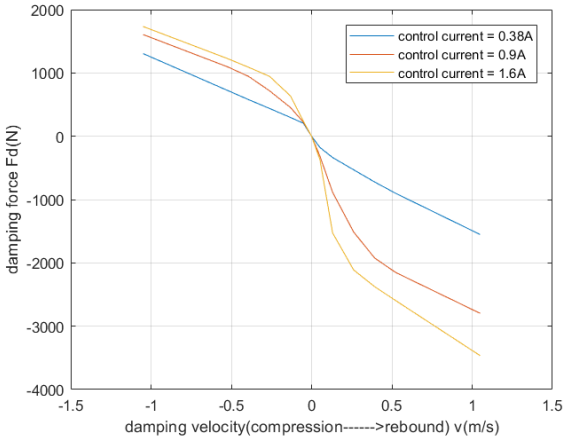

Figure 4.4: *Rear damping force vs damper velocity for different control currents for the semi-active damper*

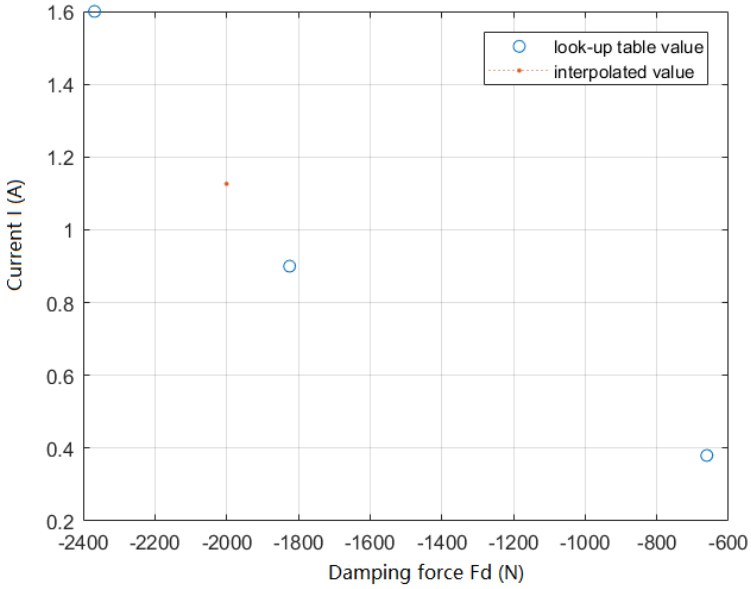

Figure 4.5: *The interpolation value of control current*

The control system flow chart is shown in Figure 4.6.

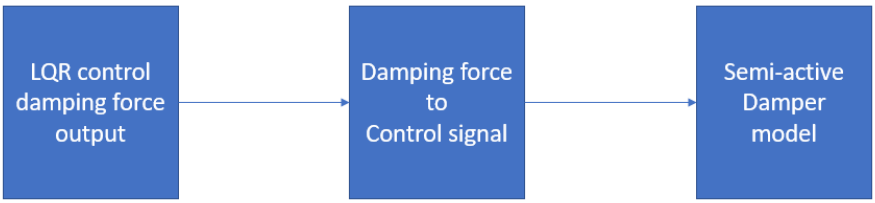

Figure 4.6: *The flowchart of the LQR semi-active suspension control*

4.3 Implementation of additional controllers

In addition to the LQG controller, two additional controllers are also implemented to compare their performance in optimizing the tire grip with the LQG control. The first one is active curve fitting control. The optimization problem behind this method is to manually test all available damping force at predefined damper velocity to find the most suitable damping force with minimum vertical force variation. The resulted curve defines the damping coefficient that can maximally optimize the vertical force variation. The second method is compression maximization control. It is inspired by the theory behind how the damping force affects the load transfer rate on the tire contact patch. The optimization problem in this method is to reduce the influence of load transfer on the vertical force variation of the tire contact patch during driving.

4.3.1 Active curve fitting

This approach is behind the thought that there exists an optimal damping force-velocity curve which can maximally minimize the wheel vertical vibrating acceleration. By sweeping the damping force at different damper velocities, it can be found that with one specific damping force, the RMS level of the wheel vertical acceleration variation is minimum. The velocity points defined for sweeping are the same as the velocity in the force-velocity curve for the semi-active damper. The interesting vibrating frequency in this project is around the wheel hob frequency, which is set to be 10 hz in the sweeping. The excitation from vertical displacement of the wheel contact point is varying to ensure the maximum damper velocity reaches the corresponding targeting value. The sweeping procedure is conducted from the car's front side to rear side and extends from the damper's static state to both directions of compression and rebound. The pseudo code of active curve fitting algorithm is shown in Algorithm 1, where F_{dfit} is the final selected damping force, F_d is the damping force in the tuning process. The generated damping force-velocity curve for fully-active suspension is also applied on semi-active damper. The simulations of the curve on both fully-active and semi-active dampers will be shown in Chapter 5.

4.3.2 Maximize compression semi-active control

The damping speed for compression and rebound plays an important role in affecting the load transfer when it comes to bumps or holes on the road. Since compression damping controls how fast the weight leaves a tire and the rebound damping controls how fast the weight is added to a tire, by controlling the damping coefficient separately for compression and rebound, the load transfer rate can be tuned for the control objective. For optimizing the road grip, the load is required to be gotten fast onto the tire in compression and to be lifted slowly from the tire in rebound. In that case, the vertical force on the tire contact patch can be maximally maintained. The maxi-compression suspension control for semi-active damper is implemented based on this principle. In this strategy, the damping force in compression is maximized by setting the maximum current into the semi-active damper and the damping force in rebound is minimized by setting the minimum current into the damper. The control structure for this strategy is shown in Figure 4.7. The controlling process can be described in Equation 4.17, where v_d is the damping velocity, I_{max} and I_{min} represent the maximum control current and the minimum control current. d_{max} and d_{min} are the corresponding maximum and minimum damping coefficient. F_d is the damping force.

$$\begin{cases} v_d < 0 : I_{max} \rightarrow d_{max} \longrightarrow F_d = -d_{max} \cdot v_d \\ v_d > 0 : I_{min} \rightarrow d_{min} \longrightarrow F_d = -d_{min} \cdot v_d \end{cases} \tag{4.17}$$

Algorithm 1 Active curve fitting algorithm

1: Initialize n=13 symmetrical damper velocity points v_d

$$v_d(n=7)=0$$

$$v_d(1)=-v_d(13)$$
$$v_d(2)=-v_d(12)$$
$$\vdots$$
$$v_d(5)=-v_d(9)$$
$$v_d(6)=-v_d(8)$$

2: Initialize the number of sweeping times M
3: Initialize damping force $F_d(1)=0$
4: Start from the static point $n=7$
5: **do**
6: Define a road amplitude so that the damping velocity reaches $v_d(n)$
7: **for** t $=1$, M **do**
8: Increase the damping force at a step size of δ

$$F_d(t+1)=F_d(t)+\delta$$

9: Simulate the system with $F_d(t+1)$
10: Measure vertical unsprung mass acceleration $a_z(t)$ and calculate $RMS(a_z(t))$
11: **end for**
12: Determine the fitted damping force F_{dfit}

$$F_{dfit}(n)=F_d(t),\quad RMS(a_z(t))=\min(RMS(a_z))$$

13: $n_{old}=n$
14: Start to test v_d points equidistantly around $n=7$ until all v_d are covered, e.g. first is rebound damping $n=7+1$, next becomes compression damping $n=7-1$
15: Initialize the damping force for the new damper velocity level.

$$F_d(1)=F_{dfit}(n_{old})$$

16: **while** $n\neq 1$

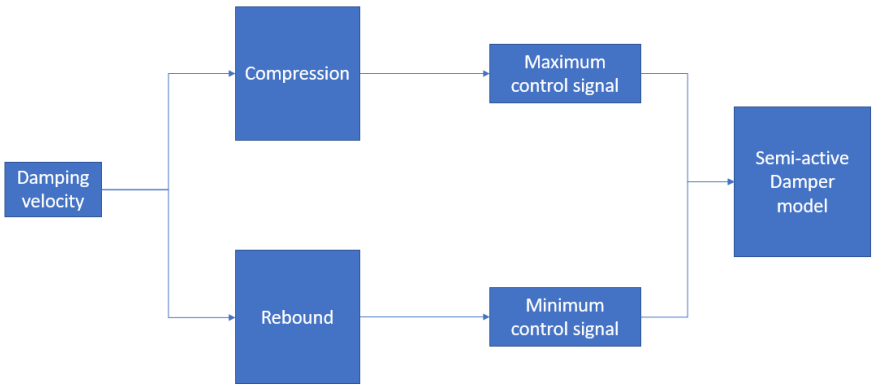

Figure 4.7: *The control structure for maxi compression semi-active control*

5 Results

This chapter presents and discusses the evaluation process of the developed controlled systems with different simulation settings. In addition to the aforementioned controllers in Chapter 4, two other passive suspensions with soft damping and hard damping are included in the simulation as a control group to the controllers. Both soft damping and hard damping are realized by the semi-active damper model. The soft damping is realized by inputting the minimum control current to the semi-active damper and in contrast, the hard damping is realized by inputting the maximum control current to the semi-active damper. Since there is no sensor for the tire vertical force, the minimization of tire vertical force variation is evaluated by measuring the wheel carrier acceleration variation. Besides, the control performance in improving the horizontal tire force attainability is evaluated by comparing the vehicle performance in emergency braking. The driving environment in simulation is provided by CarMaker and the interaction between the controlled suspension system and the vehicle model is realized through Matlab/Simulink. The car used in the simulation is provided by Volvo Cars.

5.1 Parameters for LQG controller

The design parameters for the LQG controller for both semi-active and active dampers are tuned during the simulations and the final values are presented in this section.

The covariance of the process and measurement white Gaussian noise for the system observer are chosen to be

$$R_1 = 0.1 \quad R_2 = \begin{bmatrix} 0.05 & 0 \\ 0 & 0.05 \end{bmatrix} \tag{5.1}$$

The observer gain L is calculated using the Matlab function $Kalman()$, and it is calculated separately for front and rear quarter-car model. The results are shown in Equation 5.2.

$$L_{front} = \begin{bmatrix} 0.0004 & -1.1581 \\ -0.0516 & 106.0153 \\ 0.0038 & -0.2409 \\ -0.0226 & 0.0003 \end{bmatrix}, \quad L_{rear} = \begin{bmatrix} 0.0002 & -1.2316 \\ -0.0309 & 99.1324 \\ 0.0018 & -0.1716 \\ -0.0162 & 0.0001 \end{bmatrix} \tag{5.2}$$

The weight matrix Q, R and N are separately tuned for active suspension and semi-active suspension systems according to their performance during simulations. As discussed in Chapter 4, the penalization for state errors mainly focus on the tire deflection $(Z_u - Z_r)$ and suspension deflection $(Z_s - Z_u)$, as well as the velocity of the unsprung mass. But during the tuning process, the penalization of the deflection signals is found not so effective compared to that of the derivative signals. So more weights are given to the second and forth states. The final value for the weight matrices for the active suspension are chosen as follows:

$$Q = \begin{bmatrix} 1 & 0 & 0 & 0 \\ 0 & 170000 & 0 & 0 \\ 0 & 0 & 1 & 0 \\ 0 & 0 & 0 & 100000 \end{bmatrix} \quad R = 0.01 \quad N = \begin{bmatrix} 0 \\ 0 \\ 100 \\ 0 \end{bmatrix} \tag{5.3}$$

Similar to the tuning process of the active damper, the final weight parameters for the semi-active damper are chosen to be:

$$Q = \begin{bmatrix} 1 & 0 & 0 & 0 \\ 0 & 400000 & 0 & 0 \\ 0 & 0 & 1 & 0 \\ 0 & 0 & 0 & 200000 \end{bmatrix} \quad R = 0.01 \quad N = \begin{bmatrix} 0 \\ 0 \\ 110 \\ 0 \end{bmatrix} \tag{5.4}$$

5.2 Results for active curve fitting

The road profile used for the curve fitting is a sinusoidal road with amplitude 2 cm, spatial frequency 10 Hz. The generated damping force-velocity curve for both front and rear suspension systems are shown in Figure 5.1 and Figure 5.2.

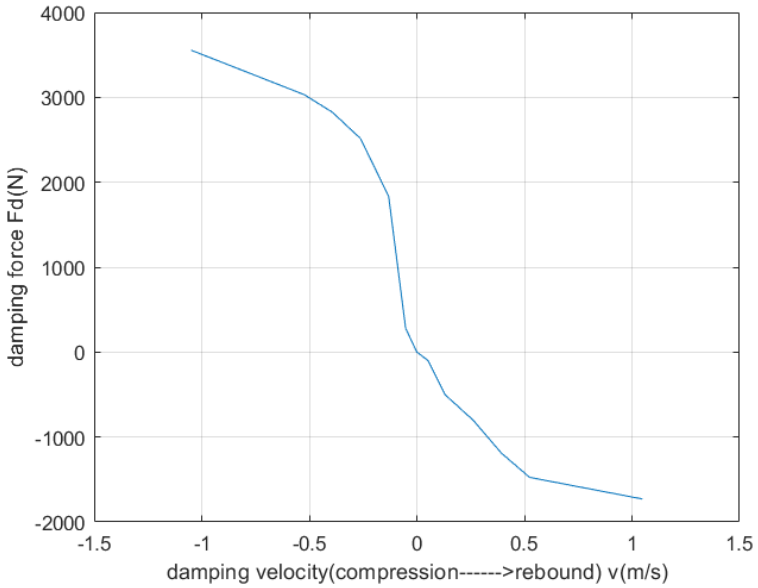

Figure 5.1: *The damping force-velocity curve for front suspension system*

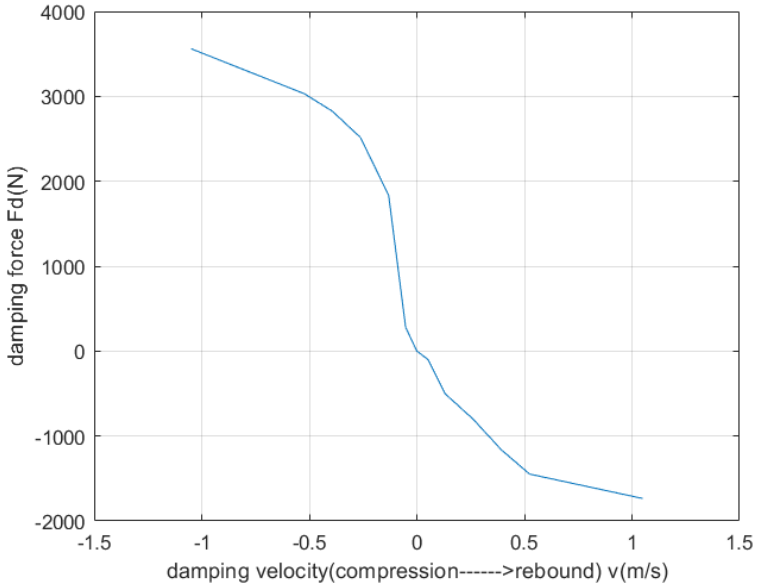

Figure 5.2: *The damping force-velocity curve for rear suspension system*

5.3 Control performance

The performance of the LQG control, active curve fitting control and compression maximization control are evaluated in this section. The evaluation process are conducted from two perspectives to evaluate the performance of the controlled systems. Minimization of vertical force variation is considered in the first stage of evaluation. in this phase, the car with the controlled suspension systems runs on predefined roads with varying road profiles. The vibration of the wheel carrier vertical acceleration is measured to represent the force variation on the tire contact patch. In the second phase, the vehicle performance with the controlled suspension during braking is evaluated. The control performance for reducing braking distance on varying road conditions is discussed and the longitudinal acceleration during braking is measured to evaluate the control performance on the improvement of the horizontal tire force generation ability.

5.3.1 Wary road with varying frequencies

This section presents the simulation results of the controlled systems on minimizing the wheel carrier vertical acceleration. The vehicle is set to be running on a predefined road with constant velocity 70 km/h (20 m/s). The velocity is self-controlled by the vehicle driver model. The road profile used in this simulation is sinusoidal roads with varying frequencies but fixed amplitude of 2 cm. The road information is shown in Table 5.1. The spatial road plot is shown in Figure 5.3.

Length(m)	Wave length(m)	Amplitude(m)	Spatial frequency(cycles/m)
20	3.33	0.02	6
20	2.50	0.02	8
20	2.00	0.02	10
20	1.66	0.02	12
20	1.43	0.02	14
20	1.25	0.02	16

Table 5.1: Sinusoidal road profile

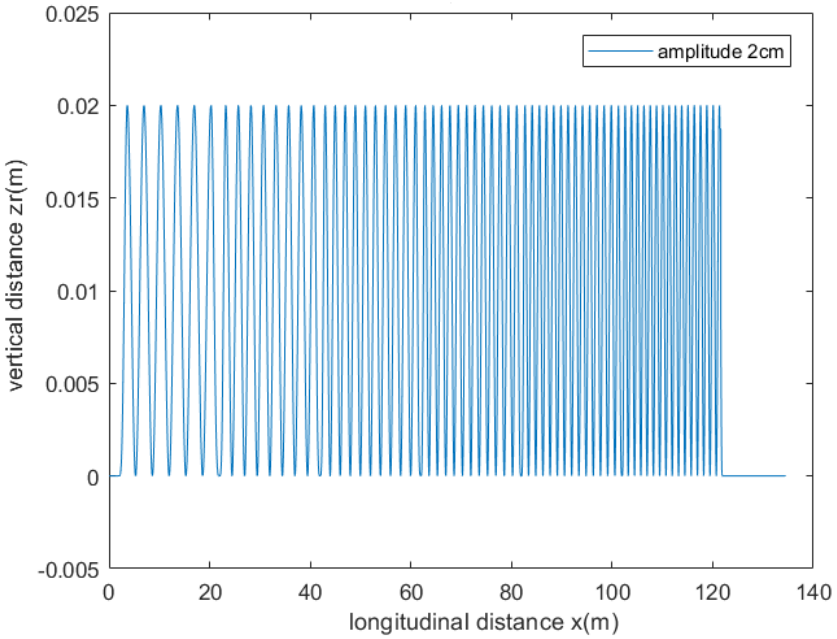

Figure 5.3: *The road profile used in the simulation for minimizing wheel vertical force variation*

The simulation results are shown in Figure 5.4. The magnitude is the vertical acceleration. This figure shows that the reduction of the vertical acceleration variation is obvious for the frequency lower than 14 cycles/m. All the developed controllers have effect on minimizing the vertical acceleration variation in this frequency range, in which the active suspension and the semi-active suspension have relatively high performance. However, when it comes to high frequency 16 cycles/m, time shifts appears and in this case, the active-curve fitting system has the largest vibration. In order to clearly see the difference in control performance among all the systems, the acceleration result at frequency 10 cycles/m and frequency 16 cycles/m are picked out and the zoom-in plots are shown in Figure 5.5 and Figure 5.6. In the case of 10 cycles/m, the active suspension performs the best in reducing the vertical acceleration variation, and it is followed by the semi-active suspension. The semi-active suspension has similar acceleration change compared to the hard suspension while the semi-active responds faster than the hard one. The soft suspension results in the largest acceleration change and the active curve fitting for semi-active system has some effect in minimizing the vertical acceleration variation. In the case of 16 cycles/m, there is obvious time shift but just from the perspective of minimizing vertical acceleration variation, the semi-active system performs the best. The hard suspension also performs well but the acceleration for the active suspension has almost the same variation as the soft suspension. The acceleration for the active curve fitting system has the largest variation in this case.

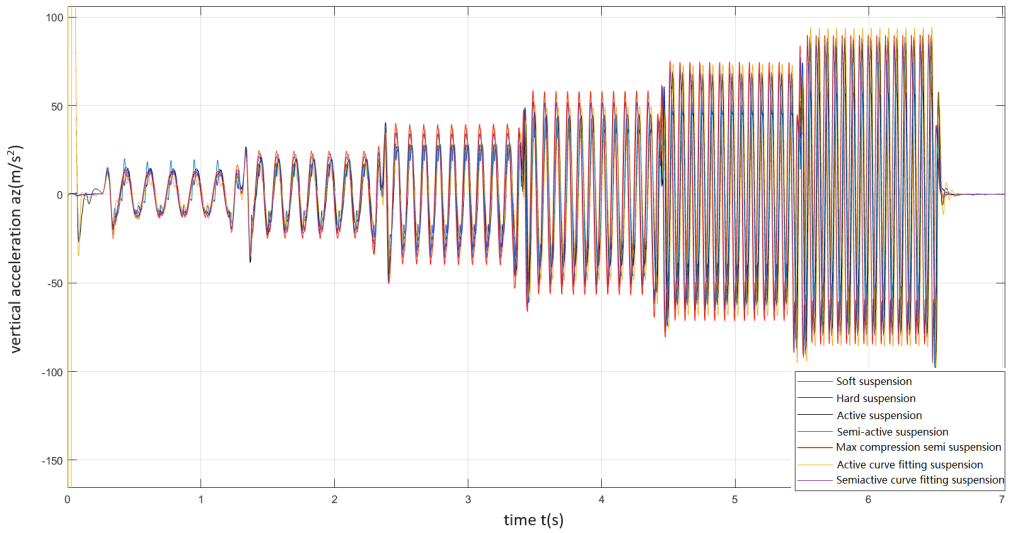

Figure 5.4: *Vertical acceleration for road profile with 2 cm, varying frequencies*

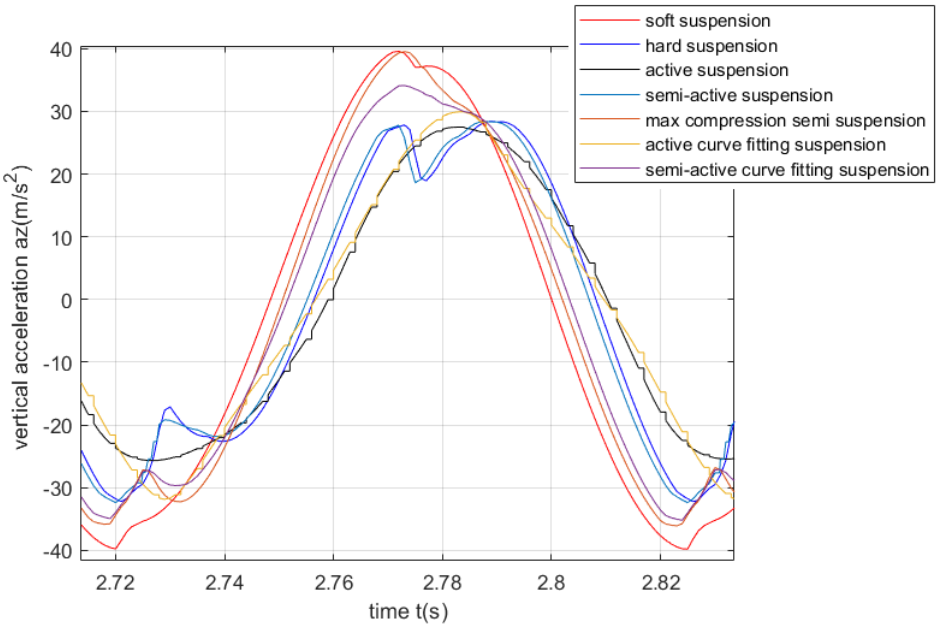

Figure 5.5: *Zoom in vertical acceleration at 10 cycles/m*

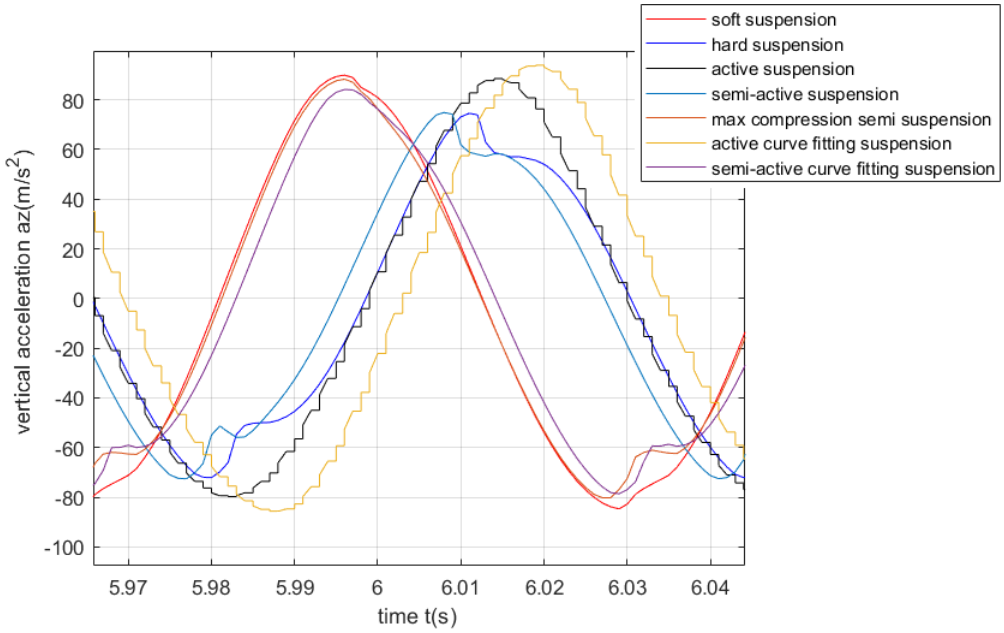

Figure 5.6: *Zoom in vertical acceleration at 16 cycles/m*

5.3.2 Braking Test

In addition to running with constant velocity, the vehicle is also tested with braking maneuver. In this section, the developed controlled suspension systems are tested under braking for a set of varying road models. There are two kinds of road profiles used to evaluate the control performance in the braking test: sinusoidal roads with constant frequencies and random roads. The spatial frequency of the sinusoidal roads varies from 8 cycles/m to 16 cycles/m, and the amplitude varies from 2 cm to maximum 10 cm in order to discuss the control performance under some extreme road conditions. The random roads are formulated by a combination of N independent cosine waves, which can be seen in the Equation 5.5. Ten spatial frequency components with randomly generated phases are considered to simulate the random road ($N = 10$). Two random roads are generated in the simulation to evaluated the control performance for the random excitation with high and low amplitude. The height of the random roads with respect to the longitudinal distance are shown in from Figure 5.7 to Figure 5.8.

$$z_r = \sum_{i=1}^{N} \hat{z}_i \cdot \cos(\Omega_i \cdot x + x_{0i}) \tag{5.5}$$

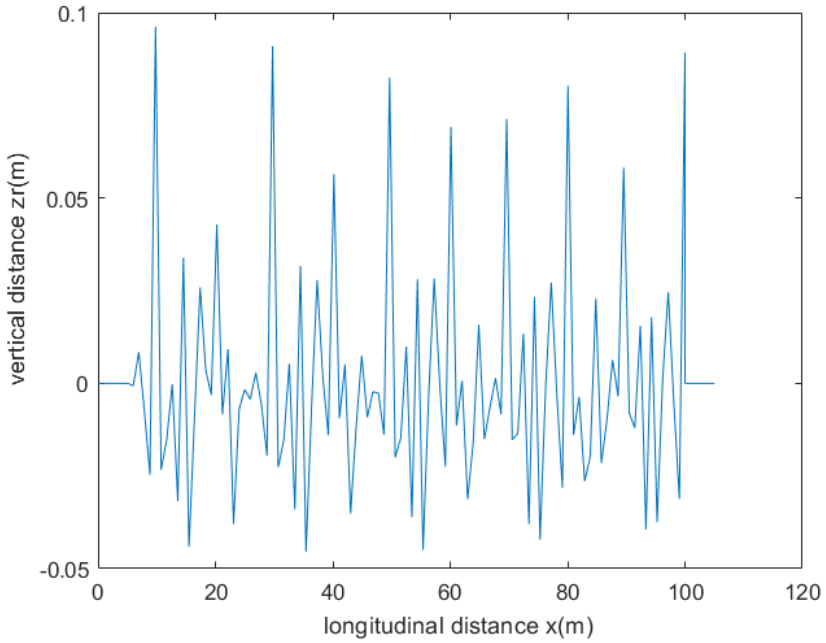

Figure 5.7: *Random road profile with high amplitude*

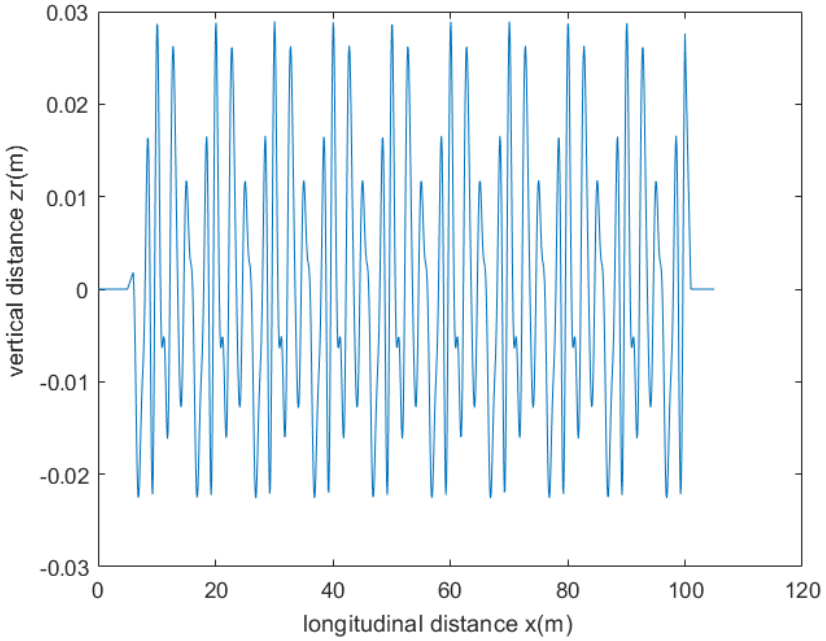

Figure 5.8: *Random road profile with low amplitude*

The car enters the testing road at an initial velocity 70 km/h (20 m/s) as well. Full-brake is applied to the car and the simulation is assumed to stop when the car speed is less than 0.001 m/s. Since the braking distance does not show significant difference for the first few seconds at relatively high velocity, in order to clearly show the difference in the braking distance, the simulation plots are zoomed in and the result is displayed from the vehicle speed of 1 m/s. Only part of the typical results which can represent the general behavior of the controllers for different roads are shown in this section and the full simulation results are presented in the appendix of this report. Since the car's speed is decreased from 70 km/h to less than 0.001 m/s during braking, the temporal frequency for the road excitation reduces from the spatial frequency to 0 Hz.

The simulation results for the road height of 2 cm, spatial frequency 8 cycles/m and 12 cycles/m are shown in

Figure 5.9 and Figure 5.10. For the spatial frequency 8 cycles/m, the hard suspension and the active curve fitting system show the shortest braking distance. The second shortest one is the semi-active system. In this case, the semi-active suspension performs better than the active suspension. The compression maximization system has the largest braking distance compared to other controlled systems. For the spatial frequency of 16 cycles/m, the hard suspension still performs the best in reducing braking distance. The braking distance with semi-active system is 3 cm shorter than that with the active system. The performance pf the active curve fitting system is not as good as that in the case with 8 cycles/m and the soft suspension still has the longest braking distance in this case. The maximum vertical suspension deflection for these two cases is 1 cm.

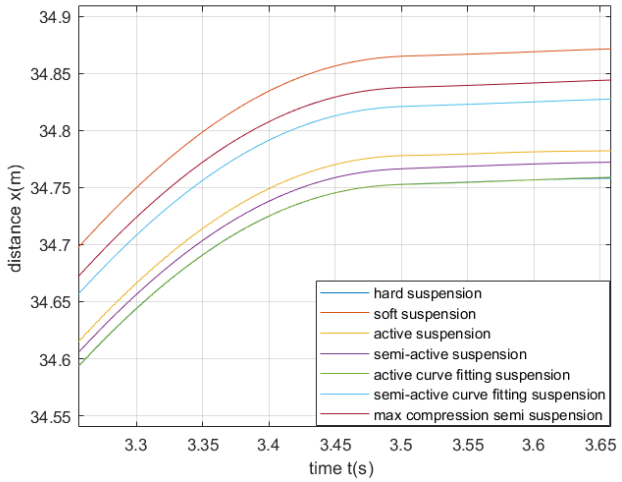

Figure 5.9: *Braking distance for amplitude 2 cm, 8 cycles/m*

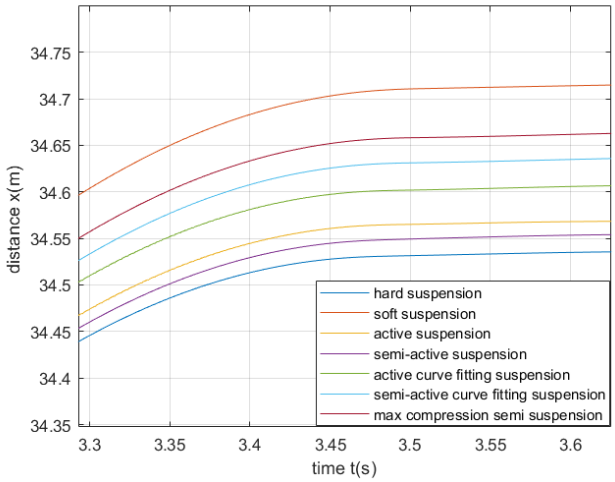

Figure 5.10: *Braking distance for amplitude 2 cm, 12 cycles/m*

The vertical unsprung mass acceleration with respect to the temporal frequency during braking for the road profile with amplitude 2 cm and spatial frequency 8 cycles/m and 12 cycles/m are plotted in Figure 5.11 and Figure 5.12. For the first case, the acceleration for the active curve fitting system has the minimum variation compared to other systems. The semi-active suspension minimizes the vertical acceleration variation for the high frequencies. But with the decrease of the temporal frequency during braking, the acceleration for the semi-active suspension shows peaks higher than that for the other systems. For the second case, the vertical acceleration is significantly minimized for the hard suspension, active suspension, semi-active suspension and active curve fitting system at the high frequencies. The semi-active curve fitting system has smaller acceleration variation than the max compression system. For the low frequencies, there is no significant difference in the acceleration value for all systems.

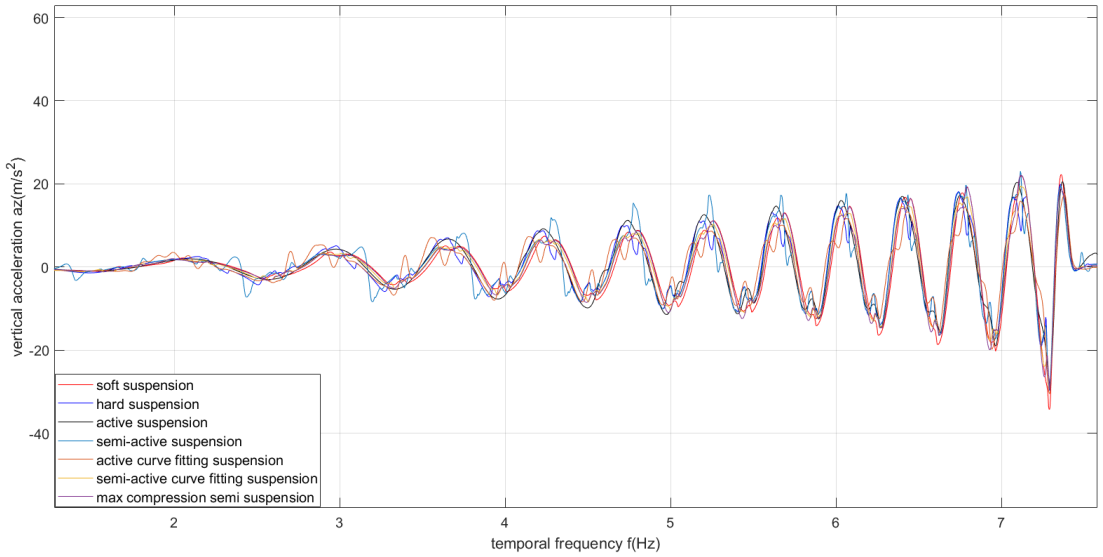

Figure 5.11: *Vertical acceleration vs temporal frequency for road amplitude 2 cm, 8 cycles/m*

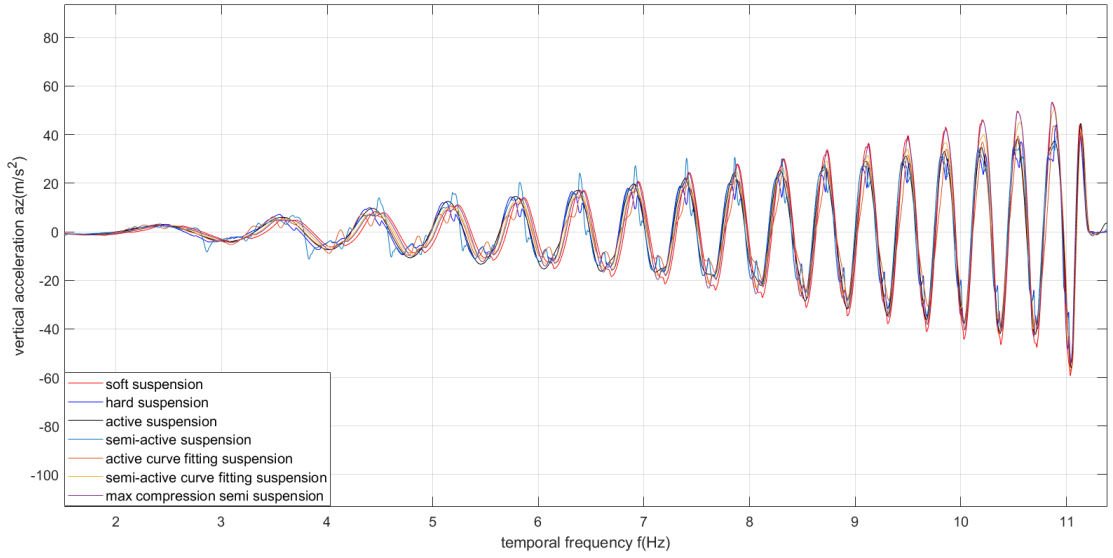

Figure 5.12: *Vertical acceleration vs temporal frequency for road amplitude 2 cm, 12 cycles/m*

The braking distance for the road with higher amplitude 5 cm and the spatial frequency 8 cycles/m and 12 cycles/m are shown in Figure 5.13 and Figure 5.14. For the spatial frequency 8 cycles/m, the braking distance for the active suspension is the shortest. The semi-active system and the hard system have close braking distance compared to each other and their performance are also close to that of the active system. The braking distances for the active curve semi-active system and the compression maximization system are 30 cm longer compared to other controlled systems. For the case where the spatial frequency is 12 cycles/m, the performance of the controllers are similar to the case of 8 cycles/m. The soft suspension has the longest braking distance for both simulations. The maximum vertical suspension deflection for these two cases is 5 cm.

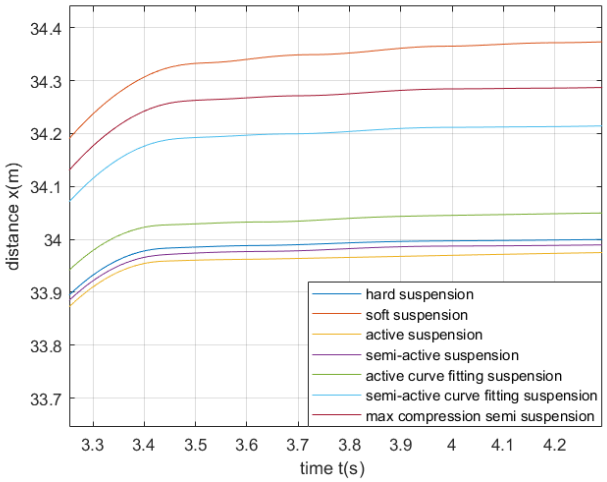

Figure 5.13: *Braking distance for amplitude 5 cm, 8 cycles/m*

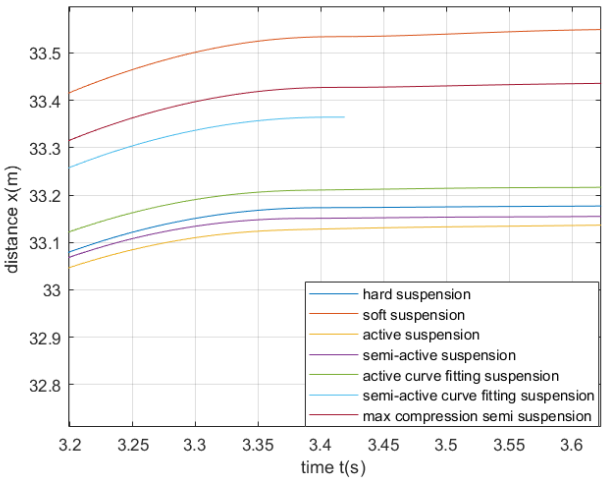

Figure 5.14: *Braking distance for amplitude 5 cm, 12 cycles/m*

The vertical unsprung mass acceleration versus temporal frequency for the road profile with amplitude 5 cm and spatial frequency 8 cycles/m and 12 cycles/m are plotted in Figure 5.15 and Figure 5.16. For the first case, the acceleration for the active suspension has the minimum variation compared to other systems at high frequencies. The acceleration variation for the semi-active suspension is also reduced compared to the active curve fitting system and the max compression system. The soft suspension has the largest acceleration variation. For the second case, the acceleration variation for the hard suspension, semi-active suspension and active suspension is largely reduced at high frequencies. But at low frequencies, the active curve fitting system performs the best compared to other systems.

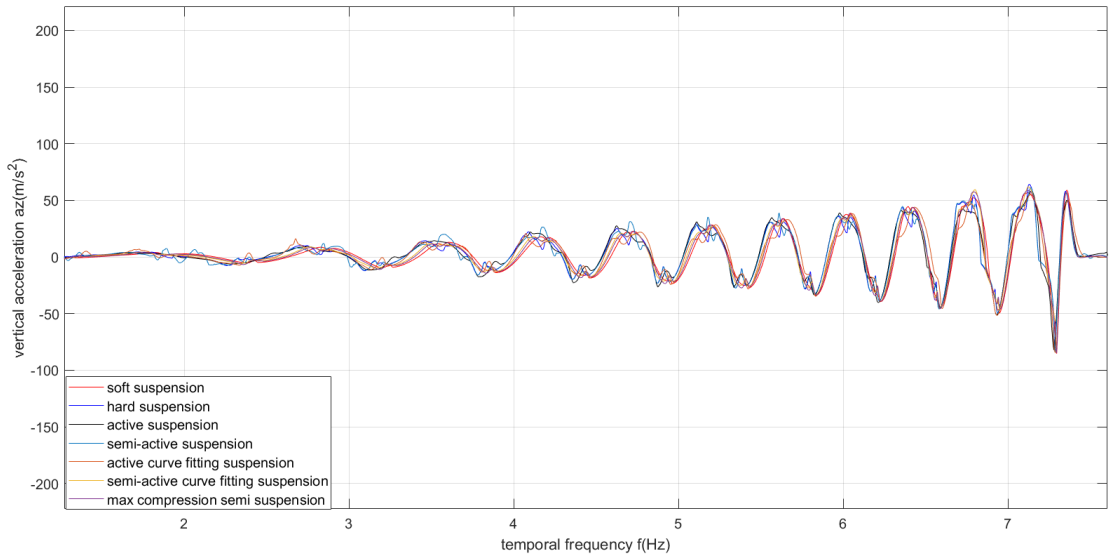

Figure 5.15: *Vertical acceleration vs temporal frequency for road amplitude 5 cm, 8 cycles/m*

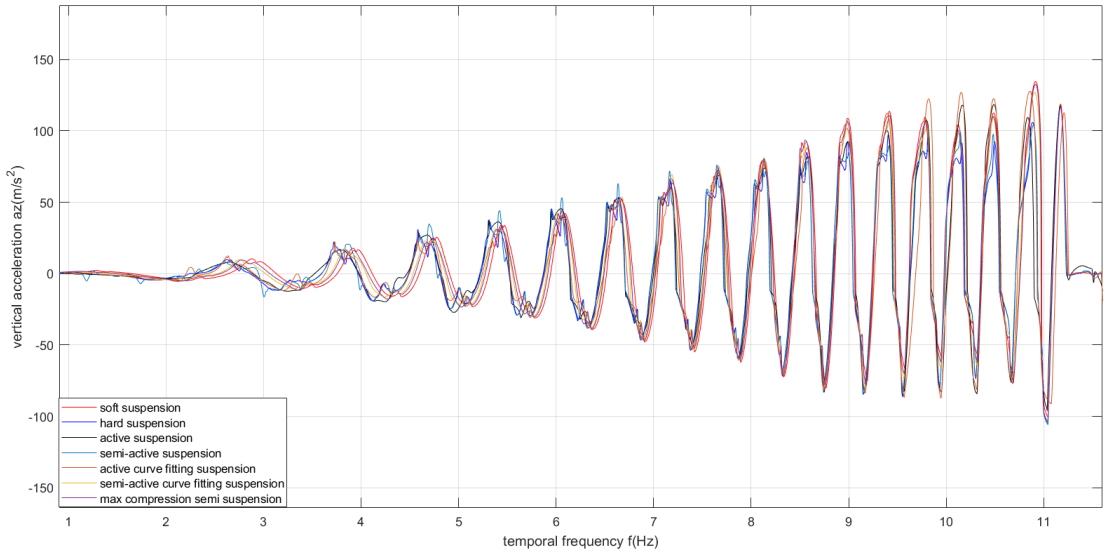

Figure 5.16: *Vertical acceleration vs temporal frequency for road amplitude 5 cm, 12 cycles/m*

The braking distance for the road height of 10 cm and the same spatial frequencies as before are shown in Figure A.1 and Figure A.2. In these two cases, the road excitation is very high, and the wheel vibration is more obvious compared to the previous simulations. For such uneven road conditions, the braking distance is largely reduced for the active suspension and the active curve fitting system has relatively good performance compared to other controlled systems. The maximum vertical suspension deflection for these two cases is 12 cm.

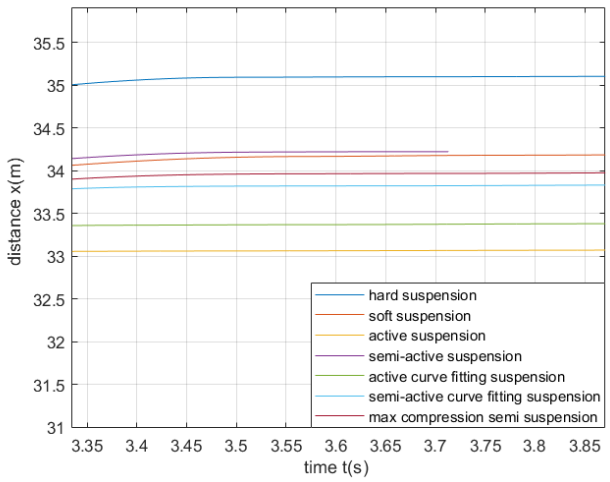

Figure 5.17: *Braking distance for amplitude 10 cm, 8 cycles/m*

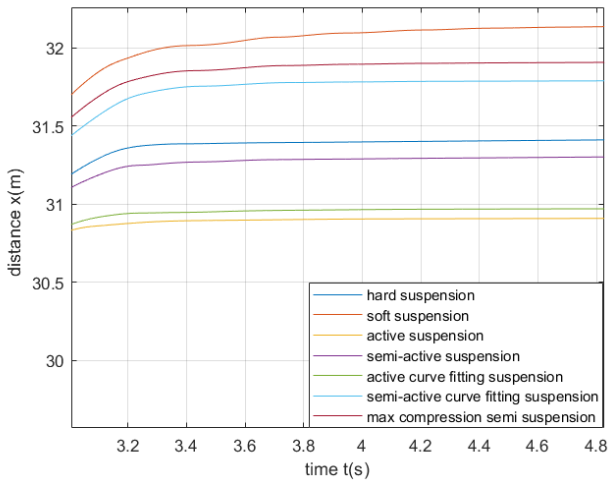

Figure 5.18: *Braking distance for amplitude 10 cm, 12 cycles/m*

The vertical unsprung mass acceleration versus temporal frequency for the road profile with high amplitude 10 cm and spatial frequency 8 cycles/m and 12 cycles/m are plotted in Figure 5.19 and Figure 5.20. Since the road is very rough, the road excitation has a greater impact on the suspension system compared to previous braking tests. There are significant shifts in the acceleration value for these two cases. Compared with other systems, it can be seen that in the first figure, the acceleration for the active suspension has minimum variation. The active curve fitting system also has a good performance in reducing the acceleration variation. In the second figure, the acceleration variation for the active suspension is largely reduced compared to other systems and the semi-active suspension has a good performance at high frequencies.

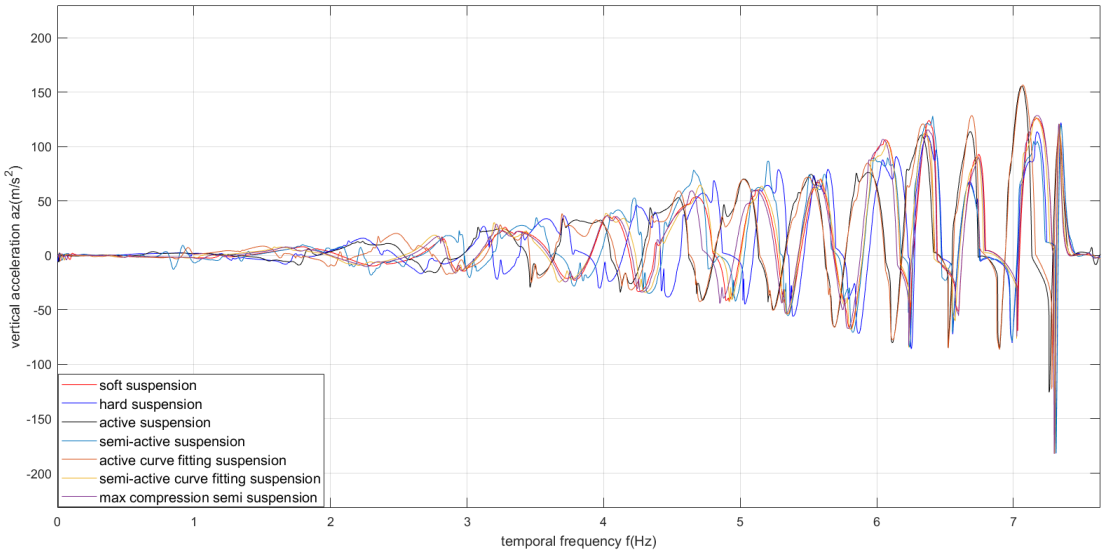

Figure 5.19: *Vertical acceleration vs temporal frequency for road amplitude 10 cm, 8 cycles/m*

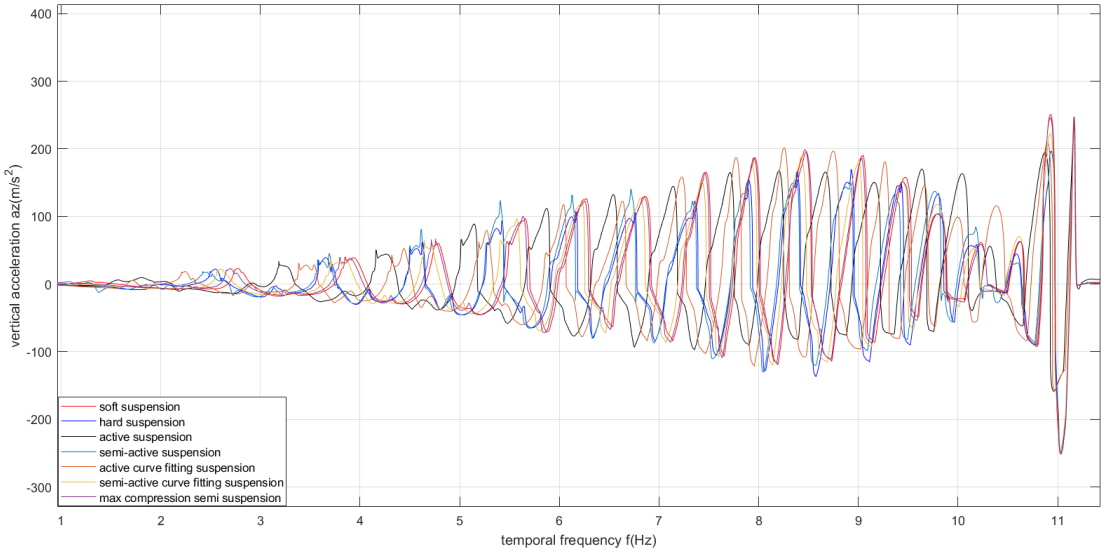

Figure 5.20: *Vertical acceleration vs temporal frequency for road amplitude 10 cm, 12 cycles/m*

In addition, this thesis also studies the braking performance of the vehicle under high frequency oscillation. The simulation results for the road with height 5 cm and 10 cm, the spatial frequency 16 cycles/m are shown in Figure 5.21 and Figure 5.22. For the excitation amplitude 5 cm, the semi-active suspension and the hard suspension perform better than the active suspension and the braking distance for the hard system is the shortest compared to other suspension systems. However, for the case with higher excitation, the active suspension performs the best in reducing the braking distance. The active curve fitting system also has an acceptable performance in this case. The maximum vertical suspension deflection for these two cases is 11 cm.

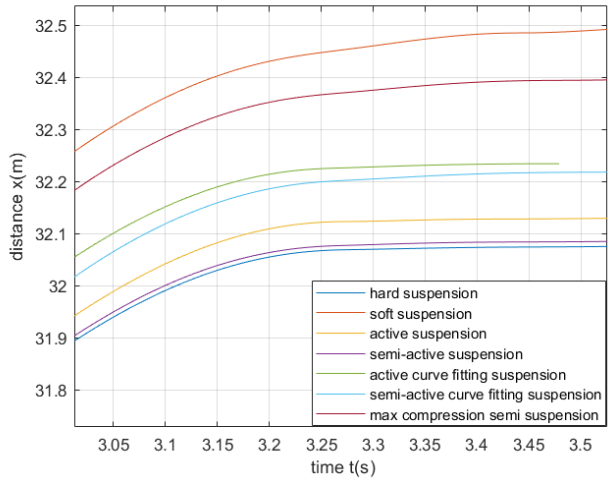

Figure 5.21: *Braking distance for amplitude 5 cm, 16 cycles/m*

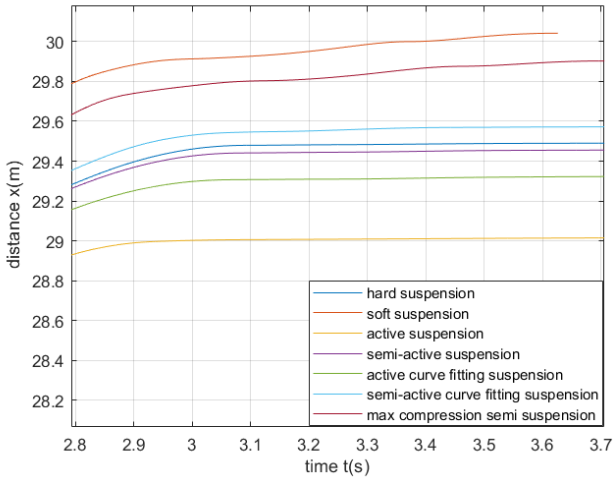

Figure 5.22: *Braking distance for amplitude 10 cm, 16 cycles/m*

The vertical unsprung mass acceleration versus temporal frequency for high spatial frequency roads are shown in Figure 5.23 and Figure 5.24. In these two cases, the amplitude of the road profile is 5 cm and 10 cm, respectively, and the spatial frequency is 16 cycles/meter. For the first case, the active suspension has a bad performance at the frequency higher than 12 Hz. The acceleration for the hard suspension has the minimum variation compared to other systems. The semi-active suspension performs better than the active suspension in reducing acceleration variation. For the second case, the vehicle hits the first bump at the temporal frequency 14 Hz and that causes a a small variation in the vertical acceleration. With the decrease of the temporal frequency, the acceleration for the active suspension has the minimum variation at frequency between 10 Hz and 13 Hz. At low frequencies, the active curve fitting and semi-active perform better than other systems.

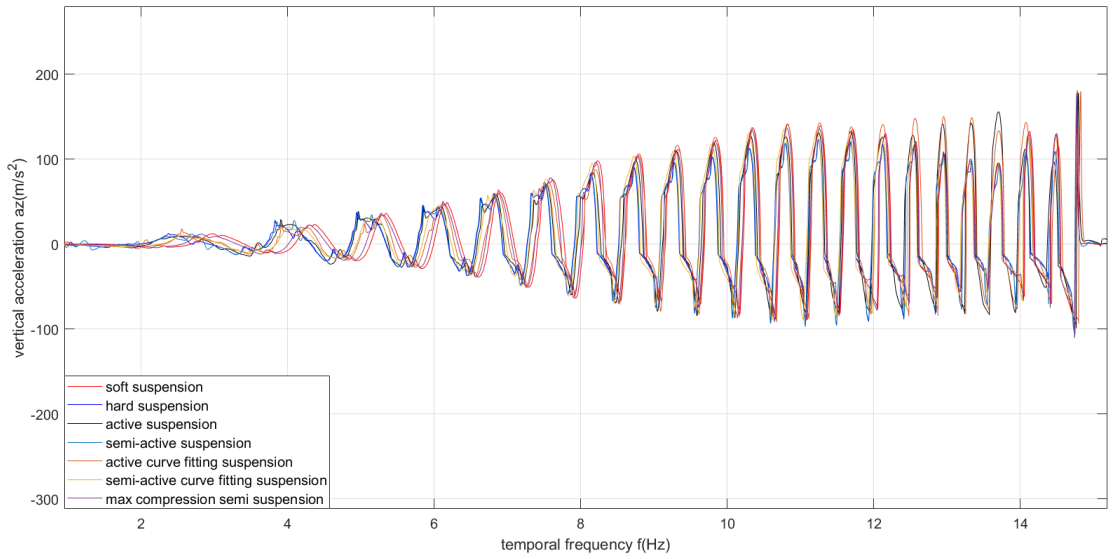

Figure 5.23: *Vertical acceleration vs temporal frequency for road amplitude 5 cm, 16 cycles/m*

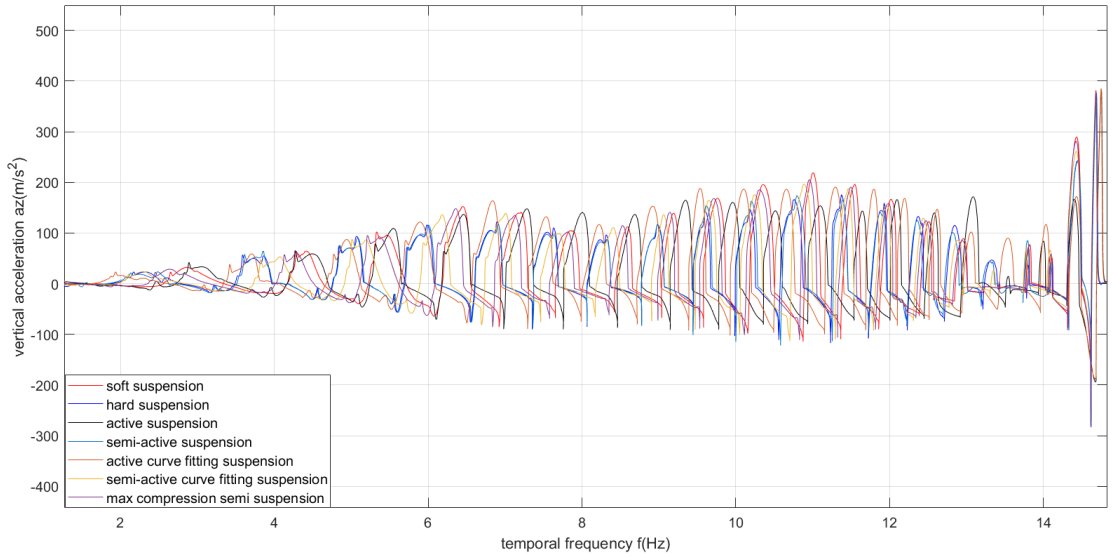

Figure 5.24: *Vertical acceleration vs temporal frequency for road amplitude 10 cm, 16 cycles/m*

The braking test results for the generated random roads are shown in Figure 5.25 and Figure 5.26. The braking distance for the active suspension is the shortest for both random roads with high and low amplitudes and the braking distance is reduced 3.2% for the active suspension compared to the longest braking distance in the case with low amplitude excitation. The active curve fitting system has the second shortest braking distance and is followed by the curve fitting semi-active system. For the case with high road excitation, the semi-active system and the active curve fitting system have similar performance to each other as they have almost the same braking distance. In both cases, the soft suspension has the longest braking distance. The tire grip under the soft suspension is the lowest compared to other suspension systems.

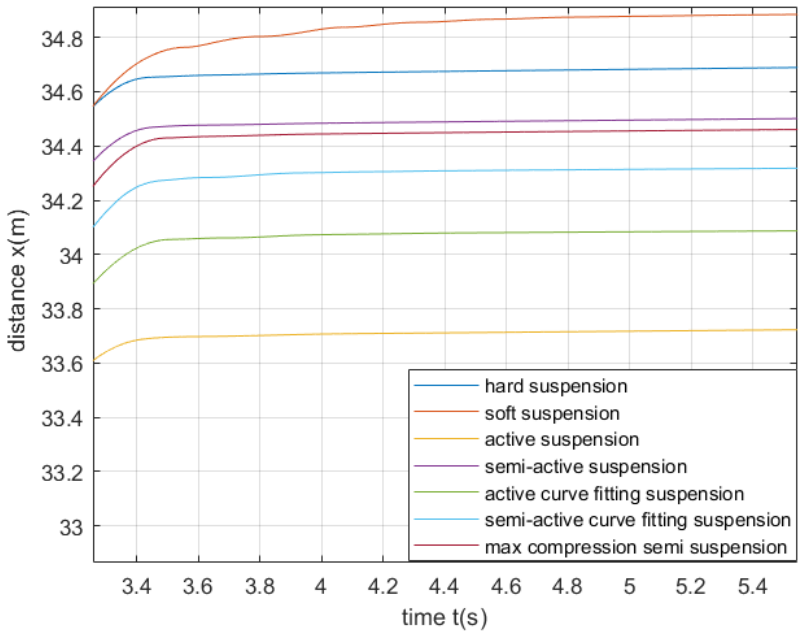

Figure 5.25: *Braking distance for random road with high amplitude*

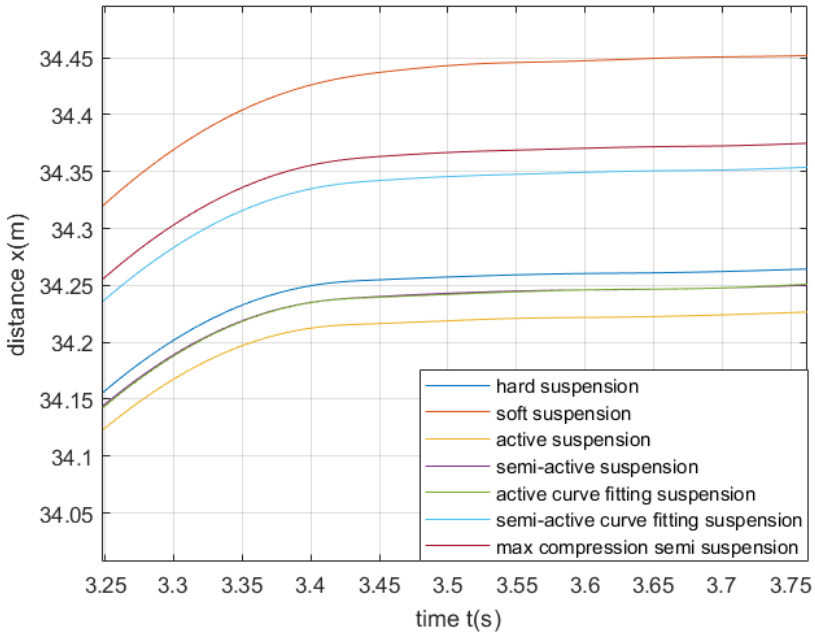

Figure 5.26: *Braking distance for random road with low amplitude*

In order to better analyze the longitudinal performance of the controlled systems during braking, the longitudinal acceleration of the vehicle during braking is measured for some typical road conditions in the simulation. Figure 5.27 shows the result for the road with amplitude 2 cm and spatial frequency 8 cycles/m. The mean value of the acceleration for the time period from 0.5 s to 1.5 s with relatively high driving speed is calculated and shown in the bar Figure 5.28. The temporal frequency range for this period is from 6.88 Hz to 4.56 Hz. The mean acceleration value for the hard suspension is the maximum compared to other controlled systems. The active curve fitting system has an acceleration value close to that of the hard suspension. The semi-active system has higher acceleration than that of the active system and the soft suspension has the minimum acceleration value. The mean acceleration value for the middle part of the braking is consistent with the final result of the braking distance. Figure 5.29 shows the longitudinal acceleration for the road with higher amplitude and spatial frequency. Similar to the case with low amplitude, the acceleration within the same time period is picked out and the temporal frequency within this period is from 10.41 Hz to 6.31 Hz. The corresponding average acceleration values are presented in Figure 5.30. The active suspension shows the maximum acceleration for the road with height 10 cm, and it is followed by the active curve fitting system. These two controlled systems also contribute to the shortest braking distance compared to other controllers in Figure A.2.

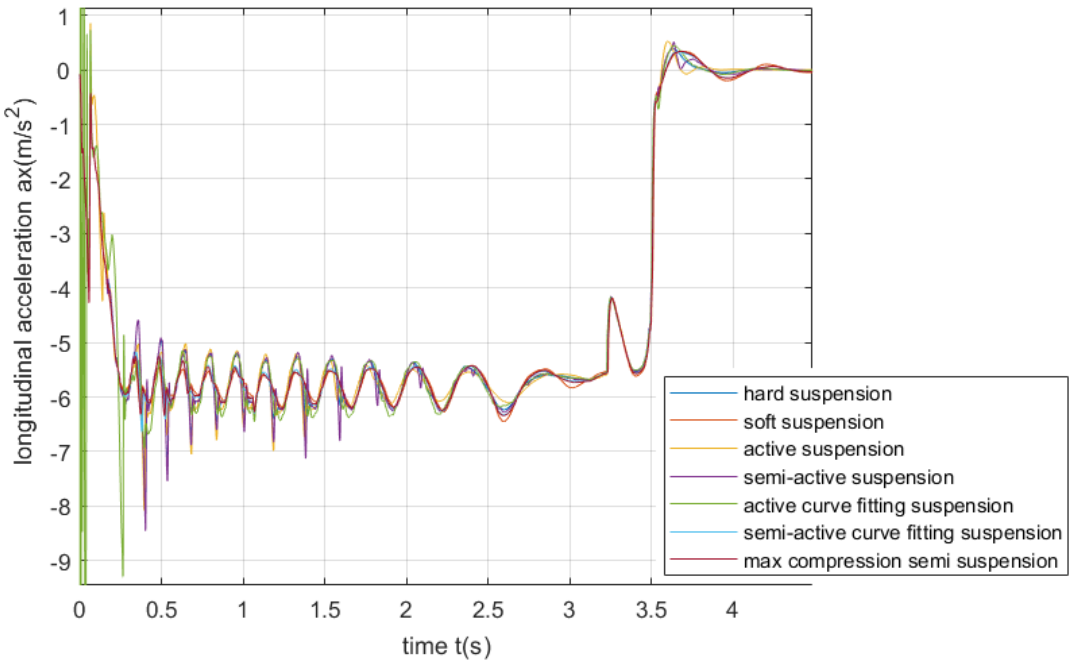

Figure 5.27: *Longitudinal acceleration during braking with road excitation 2 cm, 8 Hz*

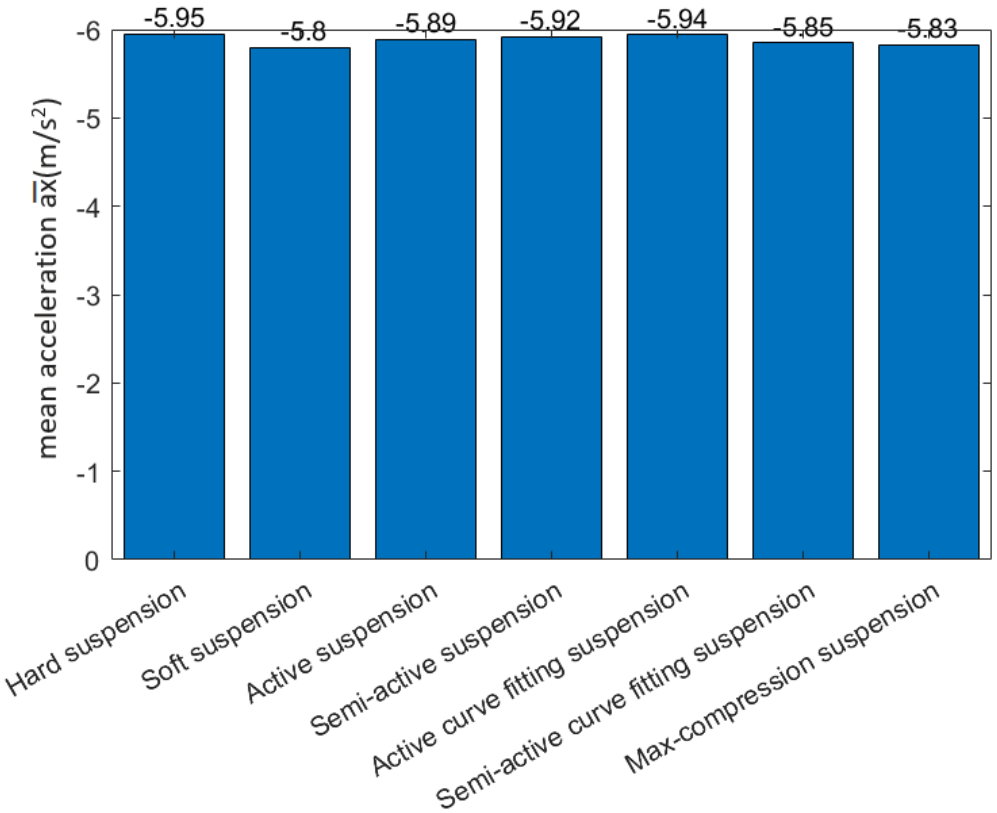

Figure 5.28: *Longitudinal average acceleration during braking with road excitation 2 cm, 8 Hz*

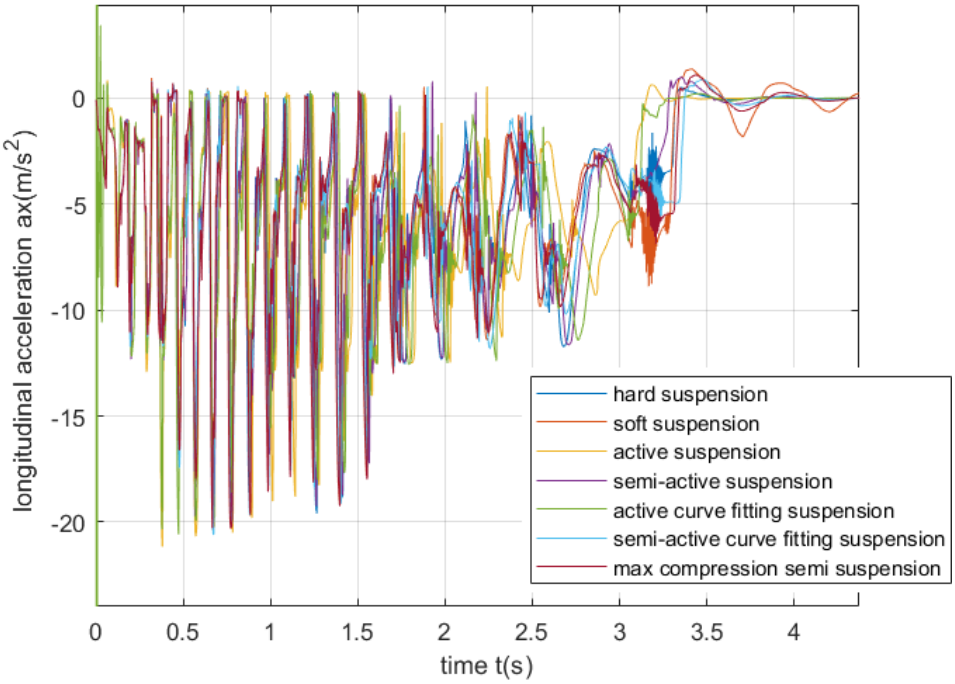

Figure 5.29: *Longitudinal acceleration during braking with road excitation 10 cm, 12 Hz*

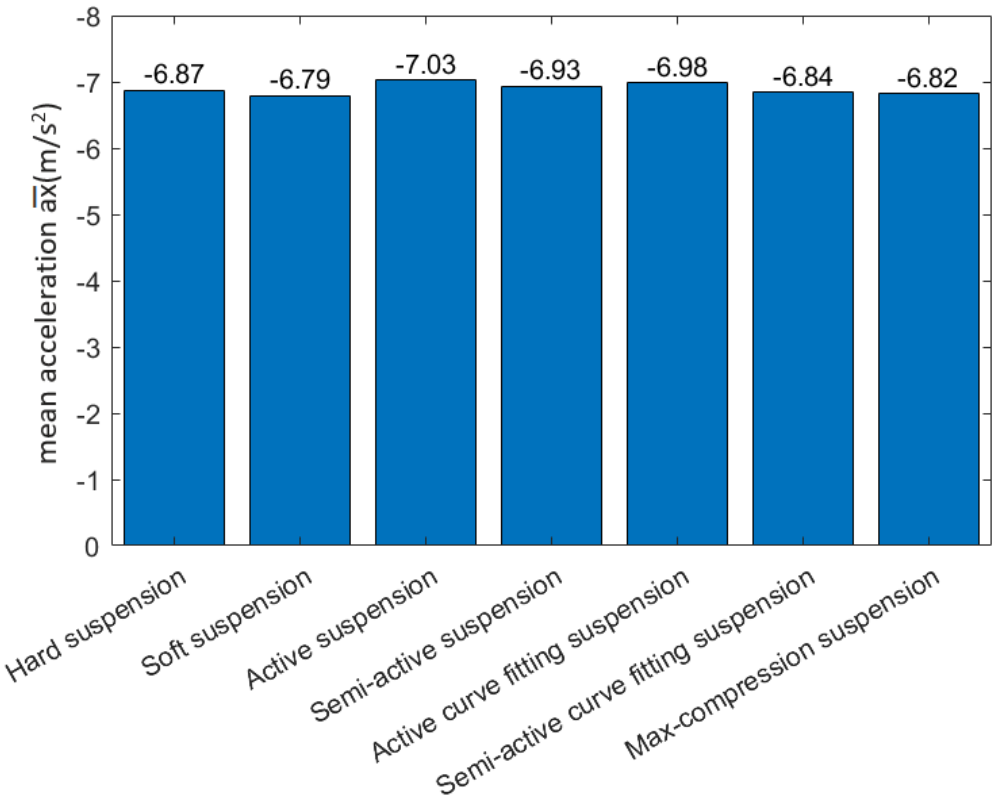

Figure 5.30: *Longitudinal average acceleration during braking with road excitation 10 cm, 12 Hz*

In addition, the longitudinal acceleration for the two random roads are also measured and the mean value for the time from 0.5 s to 1.5 s is presented in the Figure 5.31 and Figure 5.32. For the low random excitation, the active suspension shows the highest braking acceleration and it is followed by the active curve fitting system. The soft suspension has the lowest acceleration compared with other systems. The acceleration of the

semi-active curve fitting system and the max-compression system are close to each other. For the random road with high amplitude, the mean acceleration of the active suspension is significant higher than that of other systems. The second highest acceleration is from the active curve fitting system. The hard suspension has a relatively low mean acceleration for this road and the soft suspension still has the lowest acceleration value.

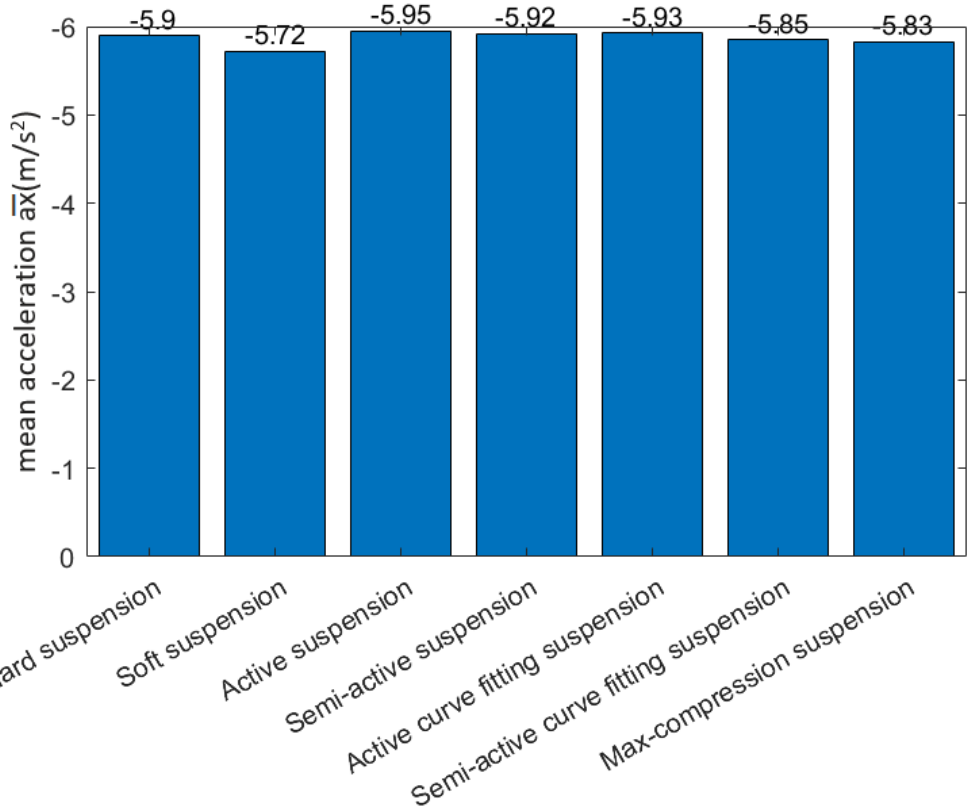

Figure 5.31: *Longitudinal average acceleration during braking with low random road excitation*

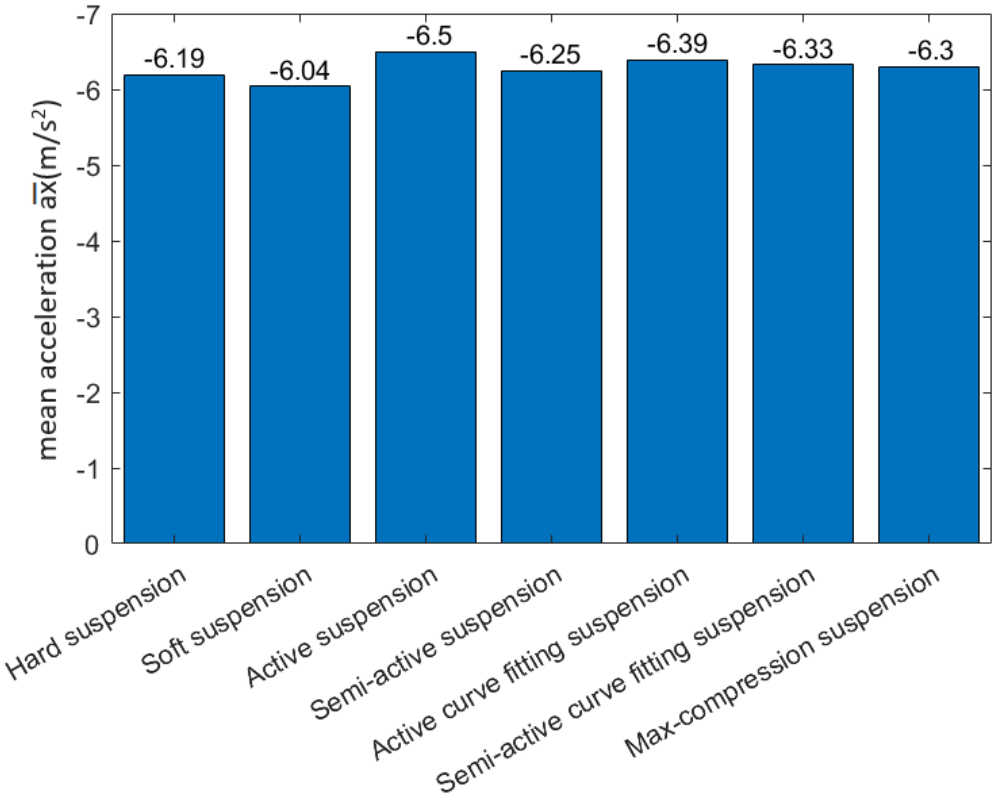

Figure 5.32: *Longitudinal average acceleration during braking with high random road excitation*

In general, the car with the soft suspension has the longest braking distance for all road conditions tested in the simulations. The active suspension system performs the best in reducing the braking distance for the road with high amplitude, while for low excitations, the hard suspension and semi-active suspension perform better. The compression maximization control has the minimum effect in reducing the braking distance compared to other controllers and in general, the suspension systems with active damper perform better than the one with semi-active damper regardless of the vibration frequency and excitation amplitude.

5.3.3 Result analysis

The LQG controllers are tuned in order to work in a wide bandwidth separately for the semi-active and active suspensions. But it is still possible that the excitation from the road surface weakens the performance of the controller. Theoretically, the active suspension should perform better than the semi-active suspension as it provides a broader range of damping force and allows energy adding to the system. However, as shown in Chapter 5, the LQG semi-active suspension performs a little bit better than the controlled active suspension for the road with low amplitude, which can be seen from the 3-5cm shorter braking distance for the car with semi-active suspension system. To analyze this problem, the actual actuator force is plotted against the expected control force for the active and semi-active dampers in Figure 5.34 and Figure 5.35. As shown in the figures, there is a significant time delay between the desired control force and the actuator force from the active damper model. But for the semi-active damper, only the last few oscillations show a little bit time delay. In order to determine the effect of the actuator on the performance of the active suspension, a braking test with ideal active control force is conducted for the same road excitation as in Figure 5.14. The simulation result is shown in Figure 5.33. The simulation result shows that with ideal control force, the performance of the active suspension is significantly improved. Therefore, it can be concluded that the dynamics of the active damper model could be the most possible reason that affects the performance of the active suspension system when the road excitation is low.

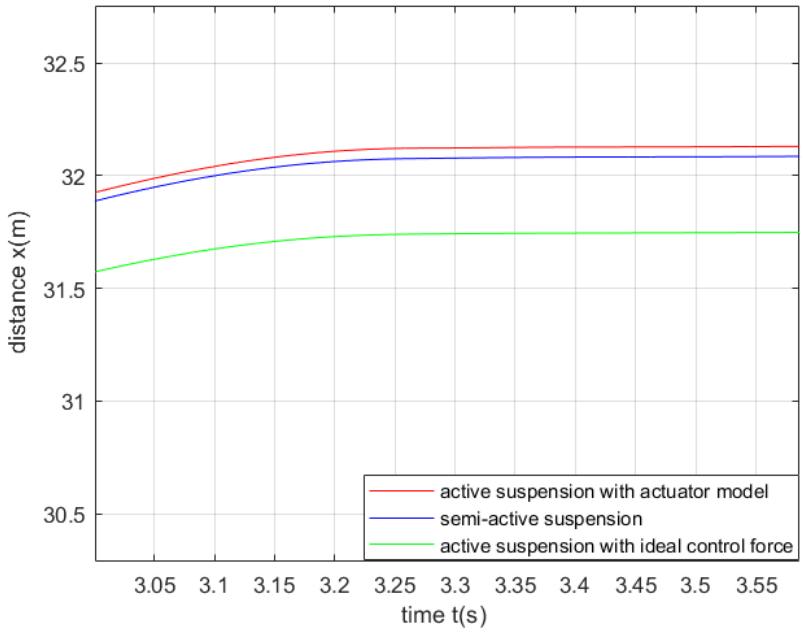

Figure 5.33: *Braking distance for amplitude 5cm, 16Hz with ideal control force for active damper*

Another possible reason affecting the performance of active damper for the high frequency input could be the limitation of the LQG control algorithm. Since the quarter-car model with suspension system is linearized around the equilibrium point, the linearized model could be no longer reliable for high frequency excitation, the operating point is far away from the linearization point. In this case, the controlled force may outrange the optimal damping force required by the system, the applied damping force thereby could not provide the value needed to minimize the vertical acceleration. However, since the semi-active damper restricts the damping force to a smaller range, it may prevent unreasonable damping applying to the system. The third possible reason that could affect the controller performance is the accuracy of the semi-active damper model, since the semi-active damper model cannot provide the required damping force according to the look-up table at high damping velocities due to its dynamic characteristics. The highest damping velocity from the operating look-up table is ± 1.049 m/s.

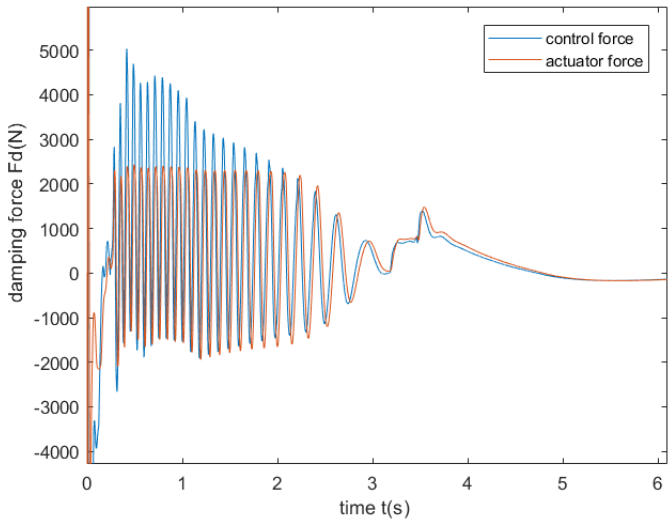

Figure 5.34: *Control force vs. actuator force for active damper*

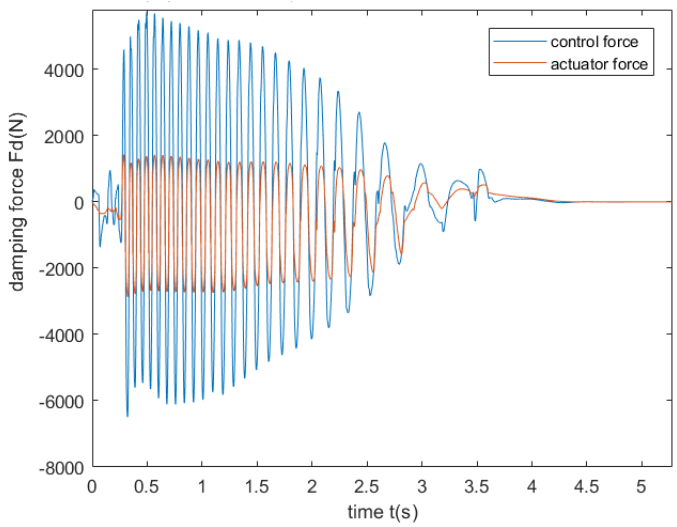

Figure 5.35: *Control force vs. actuator force for semi-active damper*

6 Discussion

This thesis aims at investigating possible control methods for both active and semi-active suspensions to optimize road grip for passenger cars. It requires the analytical model in Matlab to accurately reflect the dynamics of the quarter-car compared to the vehicle model in CarMaker. In the used tire model, the tire is modelled by a spring and a damper parallel connected to each other. Although the stiffness and the damping coefficient are chosen to be consistent with the tire used in CarMaker, in order to improve the accuracy of the model, a more complex tire model can be used. Besides, the influence of other three corners on one corner during driving is unignorable since the braking and cornering maneuvers result in load transfer which may cause extra pressure on the lower side and less pressure on the lifted side. To improve the controllers performance, a multiple input and single output system can be considered to take the parameters from other corners into account.

The actuator model for the active suspension system is an encapsulated model, which limits the possible control force it can provide to the vehicle. In other words, it limits the system's ability to follow the damping force output by the controllers. The semi-active damper is modelled by a look-up table and a first order transfer function which describe the relation between the damping force and damping velocity for different control current and the dynamics of the damper. It would be beneficial to investigate more aspects of the dampers and do a system identification for both semi-active and active dampers. With an improved damper model, the controllers can be tuned to be more adaptive to the dampers and provide a better performance.

The main discussed control strategy in this project is a linear quadratic controller. The nonlinear properties of the suspension system is not discussed in this project. Due to the fact that the linear model is unable to accurately describe the realistic system, the LQG controller shows its limitation when dealing with some extreme road conditions.

7 Conclusions

In this thesis, the semi-active suspension and active suspension systems are investigated to find possible control strategies for optimizing a vehicle's road grip. Since the road grip can be affected by the vertical suspension at the four corners, the optimization of road grip can be realized by controlling the suspension force variations. A 2 DOF quarter car model with suspension system is generated to describe the dynamics of the control plant in this project.

In order to find a proper control solution for both active and semi-active suspension systems, four different control strategies were developed. First, the LQG controller is proposed and implemented to penalize the sprung mass and unsprung mass acceleration in order to minimize the vertical acceleration variation. Beside the LQG controller, the optimal damping force-velocity curve aiming to minimize the vertical acceleration was generated to act as a criteria to guide the damping force for the active and semi-active suspension systems. Another control strategy behind the theory of maximizing the suspension force at compression and minimizing the suspension force at rebound to maximally stabilizing the vertical tire force was also implemented as a reference. The evaluation process in this project was conducted in two ways: One is by examining the minimization of vertical acceleration, the other is by comparing the braking distance of the car with the developed suspension control systems. The results show that all the developed controllers contribute to the minimization of vertical accelerations compared to the passive soft suspension. The LQG active suspension and semi-active suspension perform the best among all the controllers. The braking test with varying road excitation in amplitude and frequency show that the car with LQG active suspension has the shortest braking distance compared to other controllers for most road conditions. Therefore, it can be concluded that the LQG control for both active and semi-active suspension systems is effective in optimizing the road grip and reducing the braking distance for common wavy road conditions.

For the future work, the cornering maneuvers will be considered to investigate the control performance on the improvement of lateral tire force generation ability. The damping force can be further specially tuned at front and rear suspensions according to the braking degree to reduce the impact of load transfer on the tire vertical force variation during braking. There is also a possibility that by optimizing the actuator model for both semi-active and active damper and further tune the parameters of the LQG controllers, the performance of the controlled suspension systems could be further improved for high frequency road excitation. Also, nonlinear properties of the system could be considered in the model, and the corresponding nonlinear control strategies could be investigated to better describe the system and cover system nonlinear conditions.

References

[1] M. Abe. A study on tyre force distribution controls for full drive-by-wire electric vehicle. *Vehicle System Dynamics* (2014).

[2] V. Fors. Attainable force volumes of optimal autonomous at-the-limit vehicle manoeuvres. *Vehicle System Dynamics* (2019).

[3] T. T. Georgiou and A. Lindquist. The Separation Principle in Stochastic Control, Redux. *IEEE Transactions on Automatic Control* **58(10): 2481–2494** (2013).

[4] A. C. Hakan Koylu. Experimental design of control strategy based on brake pressure changes onwet and slippery surfaces of rough road for variable damper setting during braking with activatedanti-lock brake system. *Proceedings of the Institution of Mechanical Engineers Part D Journalof Automobile Engineering* **226(10):1303-1324** (2012).

[5] J. D. Ivan Cvok. Analysis of active suspension performance improvement based on introducing front/rear LQ control coupling. *IAVSD* (2019).

[6] J. D. Ivan Cvok. Comparative performance analysis of active and semiactive suspensions with road preview control. *IAVSD* (2019).

[7] B. Jacobson. *Vehicle Dynamics Compendium*. Chalmers University of Technology, 2017.

[8] H. Kwakernaak and R. Sivan. *Linear optimal control systems*. John Wiley & Sons, 2018.

[9] K. Lundahl. Models and Critical Maneuvers for Road Vehicles. *PhD Dissertation* (2016).

[10] B. Maclaurin. *High Speed Off-Road Vehicles - Suspensions, Tracks, Wheels and Dynamics*. John Wiley & Sons, 2018.

[11] I. Naoki. Semi-active suspension. *The technical term used in Development of Externally-Mounted Shock Absorber with Adjustable Solenoid Damping Force* **N0.55** (2017), 25.

[12] T. H. Nguyen, V. T. Vu, and M. H. D. et.al. Using the LQR control method on the active suspension system of automobiles. *10th National Conference on Mechanics and the 8th National Congress of the Vietnam Association for Mechanics* (2017).

[13] H. Pacejka. *Tire and Vehicle Dynamics*. 2006.

[14] C. P.-V. Sergio M. Savaresi. *Semi-Active Suspension control Design for Vehicles*. 2011.

[15] N. Tobias. Reducing Braking Distance by Control of Semi-Active Suspension. *PhD Dissertation* (2007).

[16] H. Xing, S. Yang, and Y. Shen. Semi-active control of vehicle seat suspension system with magnetorheological damper. *Advanced Engineering Forum* **2-3** (2004), 1067–1070.

Appendix

A Simulation result for braking test

The rest of the simulation results in the braking test are shown in this appendix. All the braking distance are shown from the vehicle speed at 1m/s. The full braking distance is also plotted here to show an example of the full driving distance. The road height for this case is 10 cm, spatial frequency is 16 cycles/m.

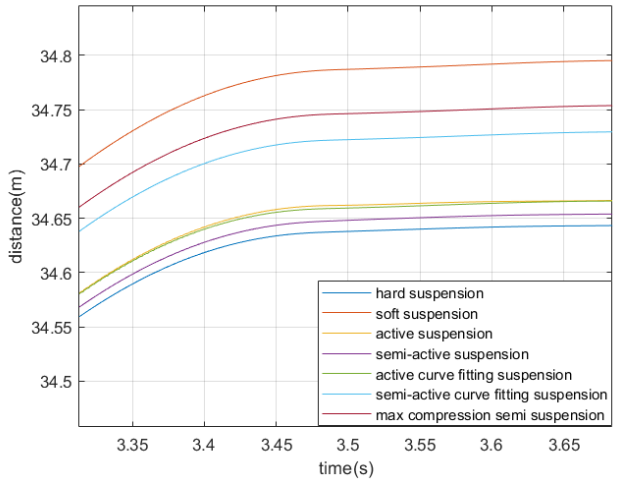

Figure A.1: *Braking distance for amplitude 2 cm, 10 cycles/m*

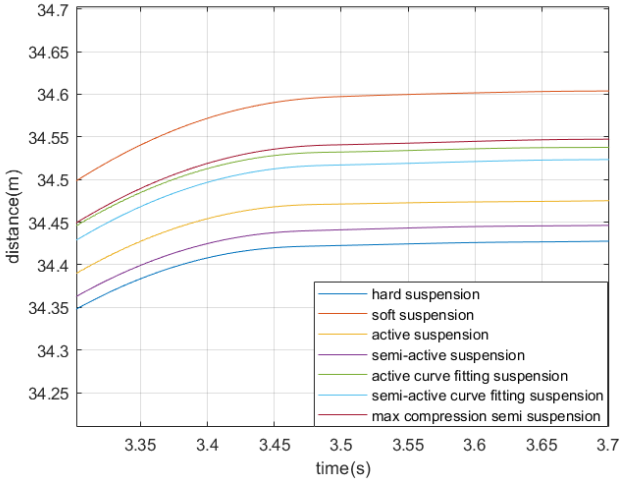

Figure A.2: *Braking distance for amplitude 2 cm, 14 cycles/m*

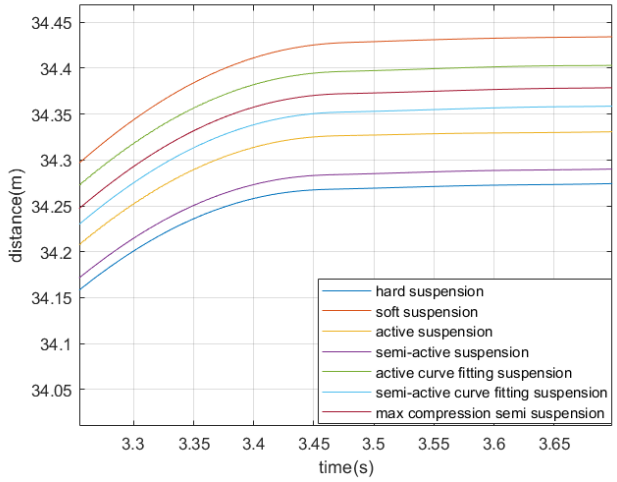

Figure A.3: *Braking distance for amplitude 2 cm, 16 cycles/m*

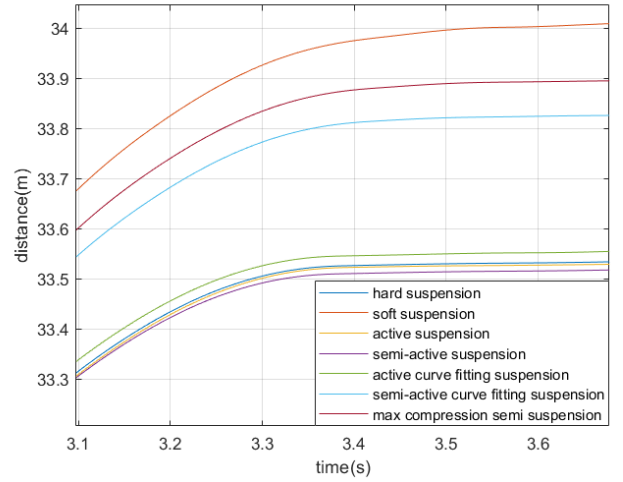

Figure A.4: *Braking distance for amplitude 5 cm, 10 cycles/m*

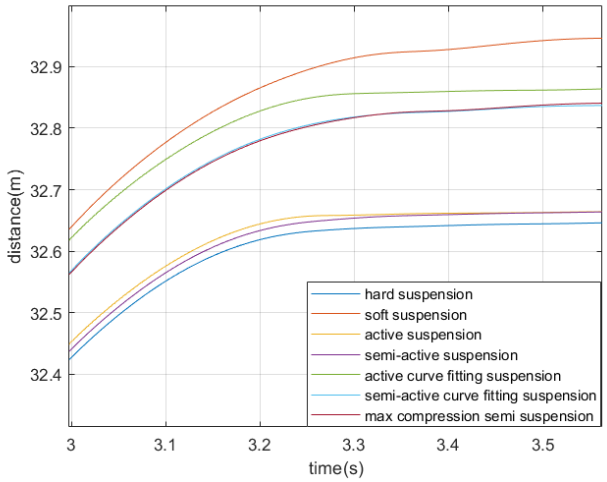

Figure A.5: *Braking distance for amplitude 5 cm, 14 cycles/m*

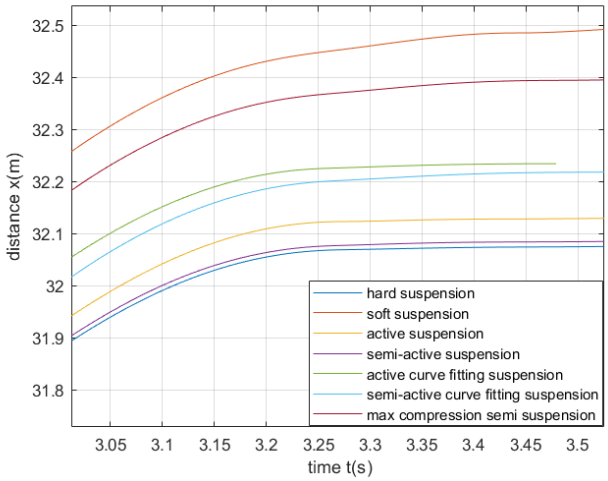

Figure A.6: *Braking distance for amplitude 5 cm, 16 cycles/m*

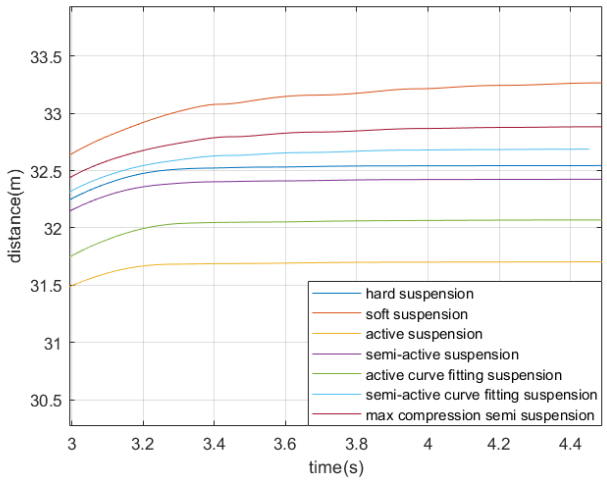

Figure A.7: *Braking distance for amplitude 10 cm, 10 cycles/m*

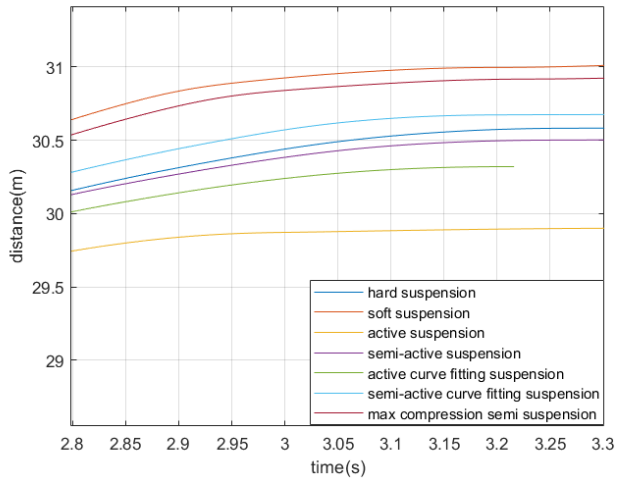

Figure A.8: *Braking distance for amplitude 10 cm, 14 cycles/m*

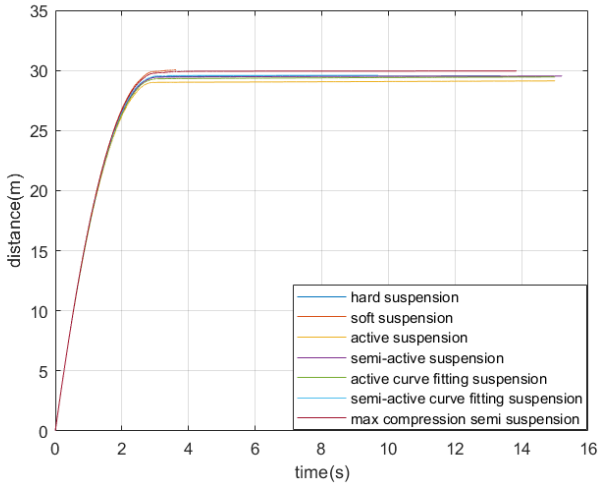

Figure A.9: *Full braking distance for amplitude 10 cm, 16 cycles/m*

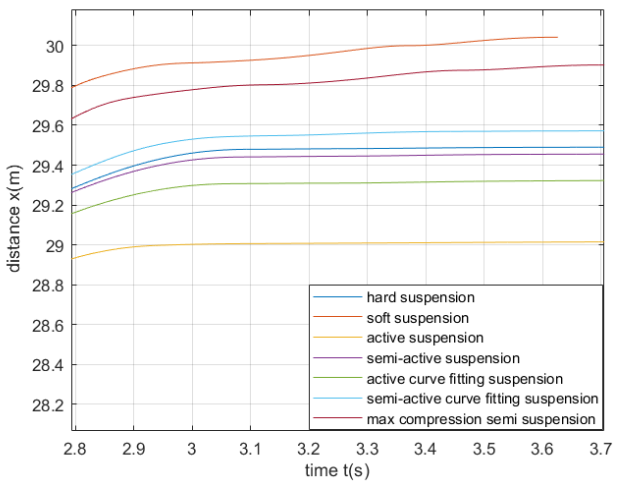

Figure A.10: *Braking distance for amplitude 10 cm, 16 cycles/m*